An optimisation study of the modified deep-hole drilling technique using finite element analyses applied to a stainless steel ring welded circular disc

Gang Zheng[1, 3*], Sayeed Hossain[1, 4], Ed Kingston[2], Christopher E Truman[1], David J Smith[1, 5]

[1] Department of Mechanical Engineering, Queens Building, University of Bristol, University Walk, Bristol BS8 1TR, United Kingdom

[2] VEQTER Ltd., Unit 8 Unicorn Business Park, Whitby Road, Brislington, Bristol BS4 4EX, United Kingdom

[3] State Power Investment Corporation Research Institute, South Park of Beijing Future Science & Technology Park, Chang Ping District, Beijing, China, 102209 (The institute was known as State Nuclear Power Research Institute)

[4] Department of Aeronautical Engineering, Military Technological College, Al Matar Street, Muscat 111, Sultanate of Oman

[5] In memory of Professor David J Smith (1951-2015) who sadly passed away on 13 Nov 2015

Abstract

A circular disc containing a partial ring weld was devised to create high levels of residual stress in a relatively small specimen. The aim of the study was to utilise the complex residual stress generated within the weld and to extend the recently developed novel application of the deep-hole drilling technique in measuring residual stresses well over yield stress. This paper presents (1) finite element analysis (FEA) simulation of the residual stresses due to partial welding in an austenitic stainless steel circular disc, (2) measurement of residual stress using non-destructive and semi-destructive techniques and (3) simulation of the semi-destructive residual stress measurement technique. Comparison is made between the FEA predicted residual stress in the weld, the measurements and the reconstructed residual stresses of the

* Corresponding author: zhenggang1@snptc.com.cn , zhenggang@spic.com.cn , zgzheng654@gmail.com

measurements. The purpose of the residual stress measurement was to validate the FEA predicted weld residual stress in the circular disc. The FEA simulation of the measurement method was used (1) to explain any discrepancy between the measured and FEA predicted stresses and (2) to further modify and extend the present deep-hole drilling technique and improve its accuracy. The close correlations confirmed the suitability of new modifications made in the deep-hole drilling technique to account for plasticity when measuring near yield residual stresses present in a component.

Keywords
Ring weld, residual stress, deep-hole drilling (DHD), plasticity, finite element method, neutron diffraction technique

1. Introduction to residual stress and measurements

Residual stresses are self-equilibrating internal stresses that remain in a body in the absence of any external loads or thermal gradients. Residual stresses can arise due to inhomogeneous deformation or from manufacturing processes and thermal treatments. Welding is a common joining process in industrial application where complex strains are accumulated leading to complex residual stresses. The presence of residual stresses is known to influence failures in structures including fatigue, creep and brittle fracture as well as structural stability, wear and corrosion behaviour. For structural integrity assessment type I, the macro residual stresses are important. The reliable method of analysing these stresses is key to accurate structural integrity assessment. In particular, to move away from decade old over-conservative structural integrity assessment. The purpose of the present study was to develop and improve the standard deep-hole drilling (DHD) residual stress measurement method with the aid of non-linear finite element analysis (FEA) and to verify by using well-established neutron diffraction residual stress measurement technique. Only the FEA simulations are presented in the present paper and measurements are provided in detail elsewhere. The DHD method provides high spatial data which increases confidence in data necessary for structural integrity assessment.

The deep-hole drilling technique relies on the measurement of the elastic distortion of a reference hole to determine the residual stresses. The reference hole is initially drilled through the component as a 'strain gauge' to obtain the distortion information

due to the original residual stress present prior to the hole drilling. Initial studies and development of the deep-hole drilling technique were carried out by Zhadanov and Gonchar (Zhdanov and Gonchar, 1978), Jesensky and Vargova (Jesensky and Vargova, 1981). Zhadanov and Gonchar examined residual stresses in steel welds in which 8mm diameter holes were drilled and 40mm core were trepanned. Jesensky and Vargova measured residual stress in steel weld, proposing to use two blind holes drilled from opposite surfaces with strain gauges attached inside the holes and on the surfaces.

1.1 Standard deep-hole drilling

The standard DHD method developed by (Leggatt et al., 1996) went through a number of further modifications and developments (Bonner, 1996a; George et al., 2000; George, 2000; Hossain, 2005; Kingston and Smith, 2003; Kingston, 2003; Poussard et al., 1995). The accuracy of the method was improved by increasing the number of measured angles from three to eight. Smith, George and co-workers (George et al., 2002; George and Smith, 2005; George et al., 2000; George, 2000; Smith et al., 2000) validated the DHD technique for use on thick steel welds to provide a reliable tool to evaluate accurately residual stress distributions and finally to compare measurements with numerical solutions. The DHD method determines the through-thickness residual stress distribution in a component by measuring the change in diameter of a reference hole that occurs when a core of material containing the hole is removed by trepanning (George et al., 2002). The steps shown in Fig. 1 include: (1) A reference hole gun-drilled through the component, (2) Accurate measurements of the initial reference hole diameter taken at a number N, of angles θ around the reference hole axis and at several increments in depth z, giving $d(\theta, z)$, (3) A core of material containing the reference hole is trepanned free of the rest of the component using a plunge electric-discharge machine, (4) After core removal, the reference hole diameter is re-measured giving $d'(\theta, z)$.

The normalised distortions $u_{rr} = (d'-d)/d$ are related to the residual stress components $\sigma_{xx}(z)$, $\sigma_{yy}(z)$ and $\sigma_{xy}(z)$ in the plane normal to the reference hole axis. Elasticity relates the deformations occurring at a hole in a finite- thickness planar-infinite plate subjected to remote planar stress components assumed to be constant through the plate thickness. The unknown stress components are calculated from the measured normalised reference hole distortions using a least squares analysis:

$$\{\sigma(z_i)\} = -E\left(M^T M\right)^{-1} M^T u_{rr} \qquad \ldots (1)$$

where,

$$M = \begin{bmatrix} 1+2\cos 2\theta & 1-2\cos 2\theta & -4\sin 2\theta & -\nu \\ \vdots & \vdots & \vdots & \vdots \\ 1+2\cos 2\theta_N & 1-2\cos 2\theta_N & -4\sin 2\theta_N & -\nu \\ -\nu & -\nu & 0 & 1 \end{bmatrix}$$

Kingston (Kingston, 2003) developed the deep-hole drilling technique to a further level by improving its accuracy and reliability. Some well-defined residual stressed specimens were measured both to validate the DHD technique and to classify the residual stress field, and included side punched (Mahmoudi et al., 2006) and shrink fitted specimens (Hosseinzadeh et al., 2007b). The DHD technique was successfully applied to very thick engineering components including 100mm (Brown et al., 2006), 175mm (Stefanescu et al., 2004), 300mm (Ohms et al., 2006) and 450mm thick (Hosseinzadeh et al., 2007a; Kingston et al., 2006). Furthermore it was successfully applied to locations which were difficult to access in thick components (Ficquet et al., 2005; Kingston and Smith, 2003; Wimpory et al., 2003a; Wimpory et al., 2003b). This method was applied to a variety of welded steel components to obtain the through-thickness variation in residual stresses over the past decade (Amir-Hossein et al., 2006; Bouchard et al., 2005; Ficquet et al., 2009; Goudar et al., 2011; Hilson et al., 2009; Hossain et al., 2006; Hossain et al., 2008; Hosseinzadeh et al., 2009b; Mirzaee-Sisan et al., 2007; Yaghi et al., 2010). The incremental centre-hole drilling (ICHD) technique and the deep-hole drilling were applied successfully on components as complementary techniques to obtain both the near surface and the through-thickness residual stress distributions (Gripenberg et al., 2002; Hilson et al., 2009; Mahmoudi et al., 2003). Finite element analyses (FEA) were also used to develop DHD technique further. For example, Hossain et al (Hossain et al., 2008) investigated the application of the DHD technique for use in the measurement of specimens with high triaxial residual stress.

1.2 Incremental DHD

As in all mechanical strain relief techniques, the DHD technique also suffers from plastic relaxation during material removal in the trepanning step when measuring residual stresses in components containing tri-axial residual stresses (Bin, 2009; Hossain, 2005; Mahmoudi et al., 2009a; Mahmoudi et al., 2007) of high magnitude.

Hence, the distortion of the reference hole on completion of trepanning through the thickness cannot represent the original residual stress field when plastic deformation occurs. New developments were made to account for the influence of plasticity on the accuracy of the deep-hole drilling method. Mahmoudi et al. (Mahmoudi et al., 2009a; Mahmoudi et al., 2007) proposed an incremental deep-hole drilling (iDHD) technique to measure near yield residual stress distributions. They carried out a numerical study of the deep-hole drilling technique applied to the case of a cylinder subjected to equibiaxial tensile loading. The behaviour of an aluminium alloy with E of 72GPa and yield stress of 420MPa were assumed in the model and the dimensions are shown in Fig. 2 (a). The diametral distortion at a point 25mm below the surface of the cylinder was monitored as the simulated trepanning operation was carried out. Results for an applied stress of 100MPa results, Fig. 2 (b) show that the diametral distortion reduces to zero as the trepan passes the measurement point. The difference in diametral distortion before and after trepanning is used in the DHD calculation to measure the residual stress. For this level of applied stress the calculated value is correct. Also shown in Fig. 2(b) are results for an applied stress of 330MPa. The diametral distortions increase significantly as the trepan approaches the measurement point. As the trepan passes the measurement point, the diametral distortion reduces again but does not return to zero because of plastic strain accumulated in the trepanned core. Instead, as the trepan passes the measurement point the stresses are relieved elastically. It is therefore expected that the reduction in diametral distortion from its peak value could be used in a modified DHD calculation to provide the applied stress. This is the incremental DHD (iDHD) method.

In the iDHD method, the core is extracted in incremental steps, the diameter of the reference hole is measured between each increment giving diameters $d'j$ where j is the number of interrupted trepanning steps. The distortions due to elastic-plastic relaxation during intermediate trepanning steps are captured and used to reconstruct an approximate solution to the initial residual stresses. The changes in diameter are normalised to give normalised distortions $u_{rr\,j} = (d'-d'_j)/d'_j$ at the j^{th} trepan increment. Only a limited set of measurements along the reference hole axis can be obtained corresponding to the trepan increments. At each trepan increment the measured hole distortions are introduced into the standard DHD analysis procedure, Eq. 1 to provide stress components $\{\sigma_j(z_j)\}$ at each trepan increment j and are then compared and combined to create the finalised discrete measurement results.

Furthermore, because the trepanning is carried out incrementally, this provides an opportunity to measure the change in core length as a representation of the axial strain. A linear variable differential transformer (LVDT) is employed to measure the change in core length after each trepanning increment. The LVDT reading is found to be sensitive to the thermal variation during trepanning and therefore the saturated reading is used as the reliable value after the core is left to cool overnight at the end of each trepanning step. The iDHD method has been successfully applied to a variety of components(Hossain et al., 2012; Hosseinzadeh et al., 2009a, 2010; Kingston et al., 2010; Mahmoudi et al., 2009c; Mahmoudi et al., 2011; Robinson et al., 2010; Robinson et al., 2008).

1.3 Over-coring DHD

The over-coring DHD (oDHD) was developed with the aim of avoiding plasticity due to trepanning. Recent work (Hossain et al., 2011) demonstrated that the removal of a section of material containing the region of interest allowed the initial high residual stresses to relax elastically away from the yield surface. A new over-coring method combined with DHD technique was developed to improve the depth resolution as well as maintaining simplicity. Between steps 2 and 3 in Fig. 1, a large core is trepanned. This ensures that the initial near yield residual stresses redistribute elastically around the reference hole so that only elastic unloading occurs during final trepanning step 3. This method is called over-coring deep-hole drilling (oDHD) method. Rather than only removing one cylinder (i.e. core) of material containing the reference hole along its axis, trepanning is carried out in two steps. First, a 40mm diameter core concentric to the reference hole is extracted followed by re-measurement of the reference hole. The difference between the diameters before (d_0) and after (d') extraction permits us to determine the partially relaxed residual stresses. Finally, a 5mm core is removed from the 40mm core to completely relax the stresses in the 40mm core followed by re-measurement of the reference hole (d). The difference between the diameters before core extraction (d_0) and after 5mm core extraction (d) permits to calculate the initial residual stresses.

1.4 Neutron diffraction

The instrument SALSA (Strain Analyser for Large and Small scale engineering Applications), due to the high neutron flux of the ILL reactor was designed as a very

flexible instrument suited to a broad range of materials science and engineering applications (Pirling et al., 2006b). The region of interest in the residual strain scattering known as the sampling gauge volume can be defined by incoming and outgoing beams defined by slit and collimator size. Motorized slits are most useful for bulk measurements where rapid counting times are required and beam divergence may be less critical. The beam can be defined more precisely by radial collimators. Collimators provide low background signal and reduce surface aberrations and so are useful for near-surface or interface measurements (Hughes et al., 2006; Pirling et al., 2006b).

The neutron diffraction technique relies on Bragg's law

$$n\lambda = 2d_{hkl}\sin\theta \qquad \ldots(2)$$

where λ is the wavelength, d_{hkl} is the interplanar spacing of diffraction planes, 2θ is the diffraction angle.

At ILL the wavelength λ is constant at 1.648Å so that Eq. (2) can be written for a stress-free sample and a stressed sample

$$d_0\sin\theta_0 = d\sin\theta \qquad \ldots(3)$$

where d_0 and θ_0 are the interplanar spacing and the neutron diffraction angle respectively for the stress-free sample, d and θ are for the stressed sample. The strain is given by

$$\varepsilon_{hkl} = \frac{d - d_0}{d_0} = \frac{d}{d_0} - 1 = \frac{\sin\theta_0}{\sin\theta} - 1 \qquad \ldots(4)$$

The strain components measured by neutron diffraction can be converted to stress using the generalized Hooke's law

$$\sigma_{xx} = \frac{E_{hkl}}{(1+\nu_{hkl})(1-2\nu_{hkl})}\left[(1-\nu_{hkl})\varepsilon_{xx} + \nu_{hkl}(\varepsilon_{yy} + \varepsilon_{zz})\right] \qquad \ldots(5a)$$

$$\sigma_{yy} = \frac{E_{hkl}}{(1+\nu_{hkl})(1-2\nu_{hkl})}\left[(1-\nu_{hkl})\varepsilon_{yy} + \nu_{hkl}(\varepsilon_{xx} + \varepsilon_{zz})\right] \qquad \ldots(5b)$$

$$\sigma_{zz} = \frac{E_{hkl}}{(1+\nu_{hkl})(1-2\nu_{hkl})}\left[(1-\nu_{hkl})\varepsilon_{zz} + \nu_{hkl}(\varepsilon_{xx} + \varepsilon_{yy})\right] \qquad \ldots(5c)$$

Note that the results of the measured residual stresses by the neutron diffraction technique as well as the other DHD techniques will be provided elsewhere. The present paper only considers the FEA simulations.

2. Specimen detail

2.1 Ring welded circular disc

The ring welded (RW) specimen consisted of a disc containing a recessed multi-pass ring-weld that introduced complex residual stresses of large magnitude. An Esshete 1250 bar, 185mm diameter, 52mm thick was supplied by EDF Energy to TWI for manufacturing the ring weld sample (TWI-Report, April 2005). The blank parent material first experienced a heat treatment, followed by machining to create a groove in one surface of the disc. The groove was welded and then a final machining process was undertaken to remove the top of the weld. The detailed processes consisted of the following.

(a) The 185mm OD × 52mm thick Esshete 1250 bar, Fig. 3(a), was solution heat treated at 1080 ℃ for half an hour followed by water quenching. Thermocouples were attached to the specimen to monitor and record the temperature change during both heat treatment and water quenching. The recorded temperature data permitted comparison to be made with the present FEA predicted thermal history and tune the FEA.

(b) Following water quenching, the disc was machined to the final weld groove preparation dimension. As shown in Fig. 3(b), material was removed circumferentially from the disc to a final diameter of 160mm. The disc was machined equally from both sides to a final circular disc with an overall thickness of 35mm, and further machined to final weld preparation.

(c) Manual Metal Arc Welding (MMA) was adopted to fill the groove. Welding was carried out in the flat position, according to DIN EN ISO 6947 with the specimen supported, but not restrained. All seven weld passes were deposited in one direction but with different start/stop positions. Fig. 3(c) shows the detail of the weld passes. Transient thermocouple data were recorded during the welding to permit comparison between FEA results and experimental data.

(d) Fig. 3(d) shows the final dimension of the ring weld after welding and final machining. Due to excessive welding distortion, the outer edge of the recess was machined to a depth of 5mm, while only 4mm was machined from the inner edge of the recess. The weld was machined flat.

2.2 Material specification

The thermal and physical properties including the thermal conductivity, specific heat, thermal heat transfer coefficient (film property), thermal expansion, density, Young's Modulus and Poisson's Ratio for weld and parent materials are provided in Table 1. A summary of the mechanical properties including the true stress-strain data for weld and parent materials is provided in Table 2. All the material properties listed were temperature dependant which were directly applied to weld and parent materials in the FEA model. Fig. 4 graphically shows the mechanical properties of Esshete 1250 stainless steel for both the parent and the weld materials. The Young's modulus and the yield stress both decrease with increasing temperature. The yield stress increases with strain for the parent material below 900 ℃ whereas for the weld material the yield stress is insensitive to change in strain. The material properties for the heat affect zone (HAZ) were not applicable in the present study. The thermal and physical properties are graphically shown in Fig. 5. The density decreases with temperature until reaching 1000 ℃ where it becomes insensitive to further increase in temperature. The specific heat increases with temperature and becomes constant beyond 700 ℃. The heat transfer coefficient, the thermal expansion and the conductivity all increase with temperature for the complete temperature range between 20 ℃ and 1400 ℃.

3. Thermo-mechanical model

The modelling guidelines provided in R6 (R6-Revision4, 2009) were used for the finite element prediction and validation of the residual stresses due to the ring welding of the circular disc. The modelling details of the ring weld following the guidelines provided in Fig. 6 for steps 1 to 4 are provided below. Steps 5 to 9 are explained in later sections.

Step1: the objective is to investigate the residual stress distribution raised by the weld procedure.

Step 2: the input data include: (a) specimen geometrical and material data provided in section 2; (b) welding information on the ring weld consisting of 7 weld passes, detailed heat input data for each pass shown in Table 3 where heat input, advance rate, area, pass length, body flux, weld efficiency are all listed. Also the recorded transient thermocouple data during the welding is an important input which allows the comparison to be made with FEA results.

Step 3: finite element package ABAQUS 6.10 was adopted (ABAQUS6.10, 2010).

Step 4: the global modelling approach was chosen to represent the manufacturing and welding procedure with as much detail as possible.

- A 2D axi-symmetric model using a static heat source was adopted. Although an axi-symmetric model recovers all three directional stress components, it ignores the weld bead start/stop effect. In the ring weld manufacture, weld start/stop position for all passes other than the final capping layer were randomly positioned around the circumference so that no two layers coincided. Because the start/stop effect was not considered in this study and the practical measurements were not conducted at the start/stop location, an axi-symmetric model was suitable for this study.
- A finite element thermal model was generated for the Esshete disc after quenching, machining and weld excavation, shown in Fig. 7. After the thermal and mechanical analysis of quenching, machining reduced the disc thickness to 35mm and introduced the weld excavation, Fig. 7 stage 2(i).
- A finite element welding model containing the weld pass profile and final cap machining line was generated, as shown in Fig. 7 stage 3(i) and stage 4 and the welding thermal analysis was conducted. Before the welding mechanical analysis, the quenching stresses (stress created by quenching and machining) were applied from the quenching model to the welding model. Then a mechanical analysis was carried out to obtain the residual stress distribution.
- Final machining of the cap was carried out as shown in Fig. 7 stage 4.

3.1 Quenching simulation

The dimensions of the quenching bar shown in Fig. 3(a) include 52mm thick, 185mm diameter. A 2D axi-symmetric model of the quenching bar with the dimensions of thickness 52mm and radius 92.5mm was created as shown in Fig. 7 stage 1. Different parts were defined in the quenching model, as shown in Fig. 7 stage 2. Parts 'a' to 'e' were machined away during the mechanical analysis. The left bottom point of the model was fixed to avoid rigid body motion. Symmetric boundary conditions were applied to the left edge since the model was a simulation of one half of the disc cross-section.

3.1.1 Quenching thermal analysis

The mesh employed for the thermal analysis consisted of 1592 linear quadrilateral elements of type DCAX4 (4-node linear axisymmetric heat transfer quadrilateral). The initial temperature of the model was set to 1080 ℃ to simulate the solution heat treatment. The specimen was allowed to cool to an ambient temperature of 100 ℃ in a short time period. The boundary conditions included convective heat transfer on the outer surface with a heat transfer coefficient of 16,742 $Wm^{-2}K^{-1}$. The heat transfer coefficient was selected to ensure that predictions of specimen surface and centre temperatures during the quenching process agreed with the values recorded by experimental thermocouples as shown in Fig. 8. There was no distinct difference in thermocouple readings between the centre and the outer surface. An excellent correlation existed between the measured and the FEA predicted thermal history.

3.1.2 Quenching mechanical analysis

The mesh employed for the mechanical analysis consisted of 1592 linear quadrilateral elements of type CAX4R (4-node bilinear axisymmetric quadrilateral, reduced integration, hourglass control). Mechanical analysis of the quenching process was conducted by using transient thermal data and no external load was applied to the model. Mechanical analysis was conducted during quenching until the model reached an ambient temperature of 100 ℃, which was the same as the temperature recorded by thermocouples attached on to the sample. The residual stress distribution was obtained after this analysis.

Machining was then simulated to reduce the disc thickness to 35mm and introduce a weld excavation as illustrated in Fig. 7. The detailed dimensions are shown in Fig. 3 (a) and (b). All the machined parts were individually partitioned and assigned an element set in ABAQUS CAE and the machining was achieved by using the '*MODEL CHANGE, REMOVE' ABAQUS keyword. The machining procedure removed side part 'a', Fig. 7 stage 2 in 5 steps with 2.5mm removed at each step to simulate the machining process. Material removal in multiple steps ensured elastic-plastic stress redistribution. Secondly, 8.5mm thick material was removed at the bottom part 'c' in 3 steps. This was repeated on the top layer 'b' to reduce the thickness of the disc from 52mm to 35mm. Thirdly, the hole in the disc was removed which is marked as part 'd' and finally the weld extraction of part 'e' was removed for the preparation of welding. The final profile of the quenching model is shown in Fig. 7 stage 2(i). The effect of phase transformation on residual stress was not deemed

important for the austenitic stainless steel material. The quenching residual stress remaining in the welding preparation model was thus obtained.

3.2 Welding simulation

An axisymmetric block-dumped finite element analysis was used to simulate the welding process and predict the residual stress field. Each weld pass was deposited instantaneously as a full ring weld. In order to simplify the model each weld pass consisted of 2-3 weld beads, and each weld pass was assumed only to have one weld bead in the model. The welding model contained seven weld passes and a final cap machining line was created, Fig. 7. The dimensions of the welding model were exactly the same as the real specimen dimensions shown in Figs. 3 (c) and (d). The left bottom point of the model was fixed to avoid rigid body motion. Symmetric boundary conditions were applied to the left edge since the model was a simulation of half of the disc cross section.

3.2.1 Welding thermal analysis

The mesh employed for the thermal analysis consisted of 3952 linear quadrilateral elements of type DCAX4 (4-node linear axisymmetric heat transfer quadrilateral). The welding and adjacent regions were meshed with refined element sizes as shown in Fig. 7. Thermal boundary conditions of convective heat transfer coefficients were applied to the model. The top surface had temperature dependent coefficients ranging from 4.2 $Wm^{-2}K^{-1}$ at 20 ℃ to 13.21 $Wm^{-2}K^{-1}$ at 1400 ℃ as shown in Table 1. Fixed convective heat transfer coefficients, 7 $Wm^{-2}K^{-1}$ for the side and 3 $Wm^{-2}K^{-1}$ for the bottom were applied to the model. The model consisted of 7 weld passes. The weld beads, yet to be deposited, should be physically isolated from the rest of the model. This was achieved by initially removing all the element sets for the 7 weld passes and then activating relevant weld pass element sets as required.

A thermal model was initialised at room temperature with all the weld beads removed. A simple heat source model was adapted to simulate the welding process using the following steps, (1) the weld bead into the FEA model at a fixed temperature of 1400 ℃ was introduced and the deposited bead held at this temperature for an arbitrary period, (2) a heat flux for a period of time was applied to simulate the weld torch, (3) the specimen allowed to cool down. The heat input to each weld bead consisted of holding for a period at the molten temperature and with a heat flux. The

heat flux was directly determined from the recorded welding details provided in Table 3, i.e. heat input, advance rate, weld pass cross section area, pass length, weld efficiency. These five parameters determine the 'Reduced Body Flux' value. The final step was to remove all the input heat source and cool the specimen down to room temperature of 20 ℃.

If the heat source hold time was too long, significant errors were introduced in the temperature history and gradients, in the size of plastically deformed zone, and the final residual stress field. Four thermocouples were attached to different locations on the specimen during the welding process, and permitted comparison with the temperature-time history data exported from the FEA model. The heat source holding time and cooling time in the FEA model were adjusted to provide the best match. Fig. 9 compares the transient temperature for some typical weld passes (passes 1 and 7) between the four sets of thermocouple data and the FEA predicted temperatures.

3.2.2 Welding mechanical analysis

The welding thermal model consisted of 3592 linear quadrilateral elements of type CAX4 (4-node bilinear axisymmetric quadrilateral). The quenching residual stress was mapped onto this model before the welding mechanical analysis was conducted. The only loads imposed on the welding model were transient thermal loads calculated from the previous thermal analysis.

Final machining was later conducted to machine flat the weld top as shown in Fig. 7. The detailed dimensions after final machining are shown in Fig. 3(d). The machined parts were individually partitioned and assigned an element set in ABAQUS CAE and machining was achieved by using the '*MODEL CHANGE, REMOVE' ABAQUS keyword, the same procedure as in the quench machining. The effect of phase transformation on residual stress was not considered important for the austenitic stainless steel material. The residual stress remaining in the ring weld model was thus obtained.

4. Deep-hole drilling measurement simulation

The deep-hole drilling finite element analysis (DHD-FEA) simulation was carried out in three steps. First, the axisymmetric results were rotated through a 3D half disc as shown in Fig. 10(a-b). Second, the 3D stress and strain fields were mapped onto a 3D

deep-hole drilling FEA model shown in Fig. 10(c). Third, DHD, iDHD and oDHD simulations, as shown in Fig. 10(d), were carried out.

Fig. 10(c) also shows the model mesh used to perform the deep-hole drilling simulations. The mesh in Fig. 11 illustrates the fine mesh used for the oDHD and the iDHD simulation, where the details of the various trepanning diameters and the drilling region are clearly shown. Fig. 12 illustrates the drilling and trepanning regions. Additional boundary conditions were required on the 5mm diameter core in the deep-hole drilling simulation as shown in Fig. 13. The nodes on the 90 ° position, fixed in the radial direction, prevented the core from rotation which prevents unexpected shear stress. The second additional boundary condition included the bottom surface of the core fixed in the axial direction. This boundary condition represented the back bush in practice (Bonner, 1996b) preventing the 5mm diameter core moving in the axial direction. The simulation procedures for the DHD, iDHD and oDHD simulations exactly followed the measurement steps.

4.1 Deep-hole drilling simulation procedures

4.1.1 Standard DHD and iDHD simulation

The standard DHD and iDHD simulations were performed on the right half of the model, shown in Fig. 10(c). First, a 1.5mm diameter drilling simulation was carried out by the incremental removal of element sets defining the drilled region in 18 increments. Second, a 5mm diameter trepanning step was incrementally simulated by subsequent removal of element sets defining the trepanned region in 18 increments. As the residual stress in the weld top region was of greatest concern, the trepan depth in the weld region was kept at 1mm while in the parent material the trepan depth ranged from 3 to 5mm.

The nodal displacement at each of the 8 equal angles was resolved into the corresponding angular directions to determine the diameter displacements after the drilling and trepanning steps. Equal intervals of 22.5 ° each were obtained by meshing the drill parts with equally spaced nodes. The diameter distortions at the end of the drilling step provided the reference hole diameter and were used to compare with the changes in reference hole diameter at the end of the trepanning step. The changes in reference hole diameter were then converted into strain components from which the unknown stress components were calculated using Eq. 1.

4.1.2 oDHD simulation

The oDHD simulation was performed on the left half of the model, Fig. 10(c). The 1.5mm diameter drilling simulation was carried out the same way as the standard DHD simulation while the trepan procedures were simulated in two stages. First, the element sets for the 40mm diameter trepan were incrementally removed in 11 increments. Second, the element sets for the 5mm diameter trepan were incrementally removed in 11 increments.

The diameter changes between the drilling step and intermediate 40mm diameter trepan provided the information about the partial stress release due to the 40mm diameter trepan. The diameter changes between the drilling step and final 5mm diameter trepan step provided the information about the complete stress release and were thus used to calculate the original residual stress field.

4.2 Deep-hole drilling parametric simulation study

Standard DHD, iDHD and oDHD procedures were simulated in this study. Table 4 shows that DH1 stands for standard DHD, DH2 for iDHD and DH3 for oDHD simulation. The parameters in the deep-hole drilling simulation were the initial reference hole diameter, the trepan diameter and procedure, drilling direction, i.e. from parent to weld or vice-versa. Two parametric studies were performed as shown in Tables 5 and 6. The standard DHD parametric study first investigated the influence of the DHD start location (DH4), followed by investigating the influence of the trepanning (DH5) and drilling (DH6) procedures on the initial stress field. The study of the influence of drilling and trepanning on the initial stress field was achieved by switching the material properties between elastic-plastic and solely elastic behaviour during the drilling and the trepanning steps. The use of elastic material properties avoids plastic deformation of the reference hole during drilling or trepanning. Through comparison with a normal elastic-plastic material model the influence of drilling and trepanning can be identified, i.e. whether the drilling and trepanning procedures cause plastic deformation.

DH5 adopted a novel method to change the material properties during the simulation in ABAQUS. ABAQUS does not have the function to change material properties within a model. In order to change the material properties between the drilling and trepanning steps, material properties at two different temperatures were defined: (a) at 20℃ actual elastic-plastic material properties was defined; (b) at 20.01℃ solely

elastic material properties was defined by raising the yield stress to a very high value, i.e. 8000MPa to avoid plastic deformation. During the drilling step in DH5, the model temperature was set to 20.0℃ to use the elastic-plastic material properties. For trepanning step, the model temperature was set to 20.01℃ which corresponded to fully elastic material properties. Resetting the model temperature achieved the necessary switching of the material properties.

The oDHD parametric study focused on the influence of the trepanning size and trepanning procedures. A 1.5mm diameter drill was adopted for all four studies, the trepan size and trepanning procedures were however different. As shown in Table 6, DH3 corresponded to 40mm diameter trepan followed by 5mm diameter trepan; DH7: 40mm-17mm-5mm diameter trepans; DH8: 12mm diameter followed by 5mm diameter trepan; DH9: 17mm diameter followed by 5mm diameter trepan. The use of DH7 simulation was to investigate whether an additional trepan step (17mm) between the initial over-core (40mm) and final trepan (5mm) could improve the measurement accuracy. The simulations of DH8 and DH9 were studied to optimise the trepan size and its application to a welded geometry.

5. Results and discussions

The results from the FEA simulations are summarised by first considering the outcomes from the sample simulation including both thermal and mechanical results. Then the results from the deep-hole drilling simulations are considered and compared with the initial FEA predicted residual stress results.

5.1 Sample simulation

5.1.1 Thermal results

Both the thermal history from the FE analysis for quenching and welding provided a good representation of the experimental thermocouple data as shown in Figs. 8 and 9. The fusion boundaries for all seven passes are plotted in Fig. 14, showing the maximum temperature in the model during the deposition of each weld pass. The FEA fusion boundary is compared in Fig. 15 with the macrograph (James and Edwards, 2008) (obtained from another identical ring welded specimen manufactured in parallel to the sample in the present study). An excellent correlation exists between the observation and the FEA simulation.

5.1.2 Quenching residual stress

The contour plots of the quenching residual stress are shown on the left column in Fig. 16 for radial, hoop and axial stress components. The radial stress component was highly tensile at approximately mid thickness of the disc with a maximum value of about 460MPa. This was balanced by highly compressive stresses near the top and bottom surfaces of the disc with a maximum compressive value of about 450MPa. A maximum tensile stress of magnitude 560MPa existed in the hoop direction located a little further (about 8mm) away from the mid-radial position. Highly compressive hoop stresses (>500MPa) were present around the outer edge of the disc. A maximum tensile axial stress of magnitude 180MPa was present near the mid-radial position similar to the location of the maximum hoop stress, balanced by compressive stress of 360MPa on the outer side of the disc. As expected, the axial stress magnitude at the top and bottom of the disc was essentially zero.

All the quench induced residual stress components were significantly reduced by machining, as shown on the right column of Fig. 16. The highest radial tensile stress component was located at the bottom of the weld preparation as a stress concentration caused by the excavation. High compressive hoop stress component remained on the outer surface of the disc. The magnitude of the axial stress component was reduced by the excavation process while the maximum value was still located near the mid-radial position.

5.1.3 Welding stress

The quenching residual stresses after the excavation process were mapped onto the welding model and the welding induced residual stresses were then simulated. Fig. 17 shows the residual stress distribution through the specimen, both after welding and after machining flat the weld deposition. Machining of the weld top only affects the residual stress field locally in the weld top region and does not have any global effect. The radial stress was at a maximum beneath the final pass and was about 540MPa. Compressive residual stresses greater than 240MPa was present in the centre region of the disc. The hoop stress was fairly constant in a large zone encompassing the last pass with tensile stress magnitudes of about 730MPa. This was balanced by a 400MPa compressive stress on the outer surface of the disc. The maximum axial stress component was located in the region along the fusion boundary around the last weld pass with a magnitude of about 200MPa.

5.1.4 Residual stress validation

Neutron diffraction was conducted on the specimen to validate the simulation. The instrument used to carry out the neutron diffraction measurements included the dedicated SALSA at the Institut Laure Langevin (ILL), Grenoble France. Details of this instrument are described by Thilo et al. (Pirling et al., 2006a). The neutron wavelength and the nominal Bragg angle were 1.648 Å and 98.8˚ respectively. The diffraction peaks corresponded to the {311} lattice plane.

One comb sample was extracted through the ring weld thickness to provide the stress-free measurement. In order to achieve a high level of stress relief but at the same time simultaneously ensuring a completely filled gauge volume, the reference sample cross section was limited to 5mm×6mm. Slots cut into the stress free sample created 8 teeth on the stress-free comb and permitted the axial stresses (i.e. the through-thickness stress component) to be completely relaxed. The comb sample provided stress-free diffraction data as a function of the distance across the thickness, accounting for microstructure and micro-stresses.

Neutron diffraction was conducted at 270 ° position of the ring weld specimen. It had 12 ND measurement points through the weld until reaching the parent metal. This measurement was conducted to measure the peak stress values in the welded and transition region. The ND measured residual stresses are shown in Figure 18 and compared with the welding simulation result. Overall an excellent correlation exists, in particular a very similar trend can be seen. Some differences between the ND measured and the FEA predicted results present can be thought to be due to the start/stop effect. The start/stop effect of the weld was not considered in the present study and an axi-symmetric model was considered. The ND measured results represent the stresses over a gauge volume (usually 1.5mm×1.5mm×1.5mm). The measured residual stresses would therefore not match 100% with the simulation. Nevertheless, in the present study which focusses on the optimisation of the DHD technique the comparison shown in Figure 18 is sufficient for further investigation on the measurement simulation provided in Sections 5.2 - 5.4.

5.2 Measurement simulation

The 2D axisymmetric welding residual stress results were rotated through 180 ° into a 3D half disc and then mapped onto a 3D deep-hole drilling FEA model, Fig. 10.

5.2.1 Mapping results

In Fig. 19 the effective (von Mises) stresses and the equivalent plastic strains (PEEQ) through the thickness of the weld centre for the various models including the axisymmetric (2D), the 180 ° rotated (3D revolved) and the 3D DHD model (3D mapped) are compared. Excellent correlations are observed between all the three models. The axisymmetric model and the rotated 3D model have identical stress and strain fields. The 3D DHD model consisted of specific partitions for the DHD drilling and trepanning simulations. Small differences between the rotated 3D results and the 3D DHD model came about because the latter had a different mesh size compared to the 2D axisymmetric and the rotated 3D models.

5.2.2 Deep-hole drilling simulation results

The results from the simulations of the standard DHD, iDHD and oDHD measurement processes through the weld centre line are shown in Fig. 20. Also shown is the initial weld residual stress components. The details of the three simulations are list in Table 4, DH1 is the standard DHD, DH2 is iDHD, and DH3 is oDHD. For both the radial and hoop directions, high tensile residual stresses were present at the top of the weld and decreased sharply to compressive stresses around the weld/parent interface (15mm) followed by tensile residual stresses again. In the weld top region, the hoop stress reached a magnitude of 650MPa while the radial stress reached 450MPa.

The trepanning simulation was carried out starting from the parent side and moving towards the weld top. The standard DHD simulation initially 'measured' both radial and hoop stresses correctly for the parent side, but when the high tensile weld region was reached near the weld top the simulated 'measured' tensile stresses remained relatively low. The presence of high residual stress near and above the yield stress caused plastic deformation during the trepanning procedure. This is the main reason why the standard DHD does not reconstruct high near yield tensile residual stresses.

The iDHD simulation which accounts for plasticity and the oDHD simulation which avoids plasticity both reconstructed well the residual stresses and is shown as solid squares and open circles respectively in Fig. 20. The iDHD and the oDHD radial stresses matched well with the initial FEA stress at all locations through the weld centre. For hoop stresses, the iDHD and the oDHD methods provided results which

were in much better agreement than the standard DHD but still did not completely reconstruct the residual stresses in the welded region. There are several possible reasons for this. First, this analysis did not account for the out-of-plane through thickness stress component, the axial stress component. Secondly, the iDHD/oDHD procedures may cause additional plastic deformation during drilling or trepanning procedures. The reasons will be discussed in the following section on the parametric study of the standard DHD method.

5.3 Parametric study results

Three parametric studies were conducted. First, the standard DHD parametric study examined the influence of the direction of trepanning on the reconstructed DHD-FEA residual stresses. Second, the influence of the drilling and trepanning procedures on the initial residual stress fields was studied. Thirdly, the oDHD parametric studies were carried out to demonstrate the influence of trepanning size and procedures on the reconstructed residual stresses.

5.3.1 Standard DHD parametric study

1. Trepan direction - DH1 and DH4 were both standard DHD simulations and the only difference was the trepanning direction. DH1 was trepanned from parent material surface to the weld, while DH4 was trepanned in the opposite direction. The results are provided in Fig. 21. Although DH1 and DH4 both 'measured' the stress correctly within the parent material, neither were able to reconstruct the high tensile stresses in the welded region, particularly near the outer surface where peak initial stresses are predicted. The reconstructed stresses in the welded region for DH1was critically erroneous as the compressive stresses predicted can result in optimistic structural integrity assessment. The presence of high tensile residual stress near and above yield stress in the weld region causes plastic redistribution during the trepanning procedure. The trepanning direction only determined the position where the standard DHD failed to correctly reconstruct the stresses, it did not avoid plastic deformation. Both DH1 and DH4 were unable to reconstruct the stresses correctly when they reached the high tensile region in the weld. DH4 initially failed to reconstruct the peak stresses correctly in the highly tensile welded residual stress region, but ‘measured’ correctly again when the process reached the low stress region near the interface about 8mm from the welded surface into the disc. This demonstrated that in the presence of a

stress field near and above yield, the standard DHD is still able to correctly reconstruct the residual stress when the direction of trepanning is from a high stress region to a low stress region.

Although the iDHD technique accounts for the presence of plasticity, it provides only limited data set with reduced depth resolution and is also time consuming. Therefore, there is huge advantage in conducting both the standard DHD and the iDHD processes together. For example, by adopting the iDHD process in the region where high stress fields are expected and the standard DHD process in the low stress region, measuring the high stress correctly and obtaining more data points in the low stress region.

2. Influence of drilling and trepanning - Material properties were modified in the standard DHD simulations in DH5 and DH6 in order to investigate the influence of drilling and trepanning procedures on the initial stress field. Simulation DH5 adopted normal elastic-plastic material properties for drilling and perfect elastic material properties for trepanning. This simulation was undertaken to investigate the influence of the trepanning procedure. The results from DH5 are shown as a dashed line in Fig. 22. Compared to iDHD and oDHD results in Fig. 20, it can be seen that both the radial and the hoop stresses in DH5 match iDHD and oDHD results quite well, and suggests that the ideal elastic material properties adopted in the trepanning procedure in standard DHD simulation DH5 avoided the plastic deformation of the reference hole. This confirms that the reason for the standard DHD to fail to correctly reconstruct the initial residual stress is due to the plastic redistribution during the trepanning procedure.

Simulation DH6 adopted ideal elastic material properties for both the drilling and the trepanning procedures. This simulation was conducted to investigate the influence of the drilling procedure. The results from DH6 are shown as open circular points in Fig. 22. There is no difference for the radial stress due to the relatively low stress level. For the hoop stress component, DH6 matched very well with the initial FEA results, while DH5 did not match near the weld surface. This study shows the influence of plasticity in the drilling procedure. This also explains why the iDHD and oDHD simulation results did not perfectly match the initial FEA results in Fig. 20. Not only because the out-of-plane through thickness stress component (axial stress) was not considered in the analysis but the drilling procedure itself also influenced the initial residual stress present in the component.

5.3.2 oDHD parametric study

1. Influence of trepanning procedure - One additional trepan step, using a 17mm diameter trepan, was added between the 40mm diameter and 5mm diameter trepan steps. This study was considered to investigate whether the additional intermediate trepan step could improve the measurement accuracy. The results are shown in Fig. 23. The additional step did not improve the 'measurement'. Both DH7 and DH3 results were identical.

2. Influence of trepanning size - The core objective of the oDHD technique is to remove a section of material containing the region of reference hole and allowing the initial high stresses to relax elastically away from the yield surface. The key point is to optimise the first over-core size to (1) allow elastic relaxation of the high stresses and (2) ensure sufficient stress is relaxed during the first core extraction so that the stress can be relaxed elastically during further trepan step. The dimensions of this ring welded specimen are shown in Fig. 3(d), the width and thickness of the weld were both about 15mm. Simulation DH3 already investigated the condition of over-core of diameter 40mm, which was more than twice the weld width and thickness. Other over-core sizes investigated included 17mm diameter (DH8), slightly larger than the weld width and thickness, and 12mm diameter (DH9), less than the weld size. The results are compared with DH3 and the initial FEA results in Fig. 24. Both DH8 and DH9 generally presented similar results to those from DH3. By comparing the high hoop stress region in detail, it is found that the smaller trepan size simulation DH9 under-predicted stress values compared to DH3 and DH8 simulations. In DH9 where the 12mm diameter trepan size was smaller than the weld size may have produced plastic deformations which resulted in lower reconstructed stresses. The result suggests that the over-core size should be larger than both the width and the depth of the welding to permit an initial elastic stress relaxation.

5.4 Analysis and interpretation of the deep-hole drilling simulations

Fig. 25 shows the reference hole diameter at various angles at a depth 4.1mm below the welded surface for an elastic material model. Line A represents the reference hole diameter just after the drilling process. Line B represents the reference hole diameter after 40mm diameter trepanning. Line C represents the reference hole diameter after final 5mm diameter trepanning. The standard deep-hole drilling technique measures

the diameter distortion III, the difference between lines A and C. Distortion I, difference between lines A and B represents the strain released due to a 40mm diameter trepan. Distortion II, difference between lines B and C represents the strain released due to the 5mm diameter trepan within the 40mm diameter core. The standard DHD only has a reference hole drill with a 5mm diameter trepan step, which means that strain III is released in one step so that a large strain release is expected to cause plastic redistribution, resulting in the error in the standard DHD results. The oDHD method introduces an intermediate step of a 40mm diameter trepan over-core. The 40mm diameter trepan successfully divides the large strain relaxation III into strain release I and II, where both provide elastic relaxation only. Although the oDHD parametric studies provided different trepan sizes, the final measured strains were all between lines A and C. This is the reason why none of the oDHD parametric simulations provided any noticeable improvement. Simulation DH9 in Fig. 24 had poorer results than simulation DH8. This is because the 12mm diameter trepan in step DH9 released too much stress which resulted in some degree of plasticity in the reference hole diameter. Each relaxation step should therefore be limited to elastic relaxation only in order to ensure good deep-hole drilling results.

In order to interpret further what residual stress the deep-hole drilling technique measures, i.e. whether the technique measures the point stress distribution along the centre of the reference hole or the average residual stress within the trepanned core Fig. 26 is used to illustrate the nodes selected within the 5mm diameter core for this analysis. There are two 5mm diameter cores shown, (a) the original DHD model and (b) the model after drilling the reference hole. There are two ways to plot the initial FEA predicted residual stress value from the FEA model. A line plot through the thickness at the centre-line of the reference hole. An average of all the nodal stresses within the core to represent the stress for each depth. The results are shown in Fig. 27. The line plot of the initial FEA results through the weld centre is shown as solid line, the oDHD results are shown as dashed line. The nodal averaged stresses are shown as symbols: the averaged stresses before drilling is presented as solid triangles and after drilling as open squares. All the different analysis results match well for radial stress component. For hoop stress component however, the before drill nodal averaged stresses match the initial FE results perfectly, while the after drill nodal averaged stresses match the oDHD simulation very well. From these results, it can be concluded that the deep-hole drilling technique represents the averaged stress within

the 5mm diameter core and not simply the initial stress. This conclusion confirms the finding from the parametric study of the standard DHD where it was shown that the drilling procedure influenced the initial residual stress slightly and therefore also influenced the deep-hole drilling results.

6. Conclusions

A 2D axisymmetric model was created to study the residual stress generated by quenching, welding and machining to create a ring welded circular disc. Simulations of the standard DHD, incremental DHD (iDHD) and over-coring DHD (oDHD) methods were performed to 'measure' and reconstruct the original residual stress. The results showed that the standard DHD technique could not accurately measure high stresses close to and above yield stress. However, the iDHD technique (taking account of the plasticity) and oDHD (avoiding plastic relaxation), both provided more accurate reconstructed residual stresses. The iDHD and oDHD simulation results generally showed good agreement with the initial FEA results, though the reconstructed hoop stresses were slightly lower than the initial FEA results in the region of high tensile stresses in the welded region.

Leggatt et al. (Leggatt et al., 2007) and Hurrell et al. (Hurrell et al., 2007) demonstrated that the 2D axisymmetric analyses were expected to over-estimate the hoop stresses due to the ‘tourniquet effect’ caused by the weld deposition and treating the weld beads as complete rings. So the predicted residual stress in this 2D axisymmetric model was also expected to over-estimate the actual stresses. This is confirmed by experiments explained elsewhere (Zheng, 2013).

Studies were performed to investigate a number of parameters associated with deep-hole drilling. It was shown that the trepan direction could not avoid the error in standard DHD within the high stress region, but confirmed that the standard DHD could measure lower stress region correctly after passing from a high stress region. Elastic material properties were systematically applied to the drilling and the trepanning steps to study the effect of plasticity during initial drilling and subsequent trepanning process. A novel method was developed to change the material properties between drilling and trepanning steps in ABAQUS. The results showed that the plastic deformation during the trepanning step was the main reason for the standard DHD to fail. The slight difference between the reconstructed results and the initial FEA stress was also caused by the initial reference hole drilling procedure. Different

oDHD over-core sizes were studied to optimise the trepanning size. The studies suggested that the over-core size should be at least larger than both the width and depth of the welding to generate elastic stress relaxation. Since a weld geometry varies from sample to sample, it is instructive to use FEA simulations to optimise the over-core size before conducting an experimental measurement.

Further analysis of the deep-hole drilling simulation revealed that the deep-hole drilling method represents the average residual stress within the 5mm diameter core after drilling and not the initial stress field present before drilling. This conclusion confirms the finding in the parametric study of the standard DHD where the drilling procedure influenced the initial residual stress slightly and influenced the deep-hole drilling results. However, this effect was not significant when the level of residual stress was low.

7. Acknowledgement

The authors are grateful to EDF Energy for supplying the ring welded circular disc for this study and to ILL for the use of the instrument SALSA for the residual stress measurement by neutron diffraction.

References

ABAQUS6.10, 2010. Hibbit Karlson and Sorrensen (Hks) UK Ltd, Warrington, Cheshire.

Amir-Hossein, M., Christpher, A., Christopher, E.T., Ali, M.-S., David, J.S., 2006. Generating Well Defined Residual Stresses in Laboratory Specimens. ASME Conference Proceedings 2006, 631-639.

Bin, S., 2009. The calibration and measurement of residual stresses by the deep hole drilling technique. PhD Thesis, University of Bristol, Bristol, UK.

Bonner, N.W., 1996a. Measurement of residual stresses in thick-section steel welds. PhD Thesis, University of Bristol, Bristol, UK.

Bonner, N.W., 1996b. Measurement of Residual Stresses in Thick Section Welds. PhD Thesis, University of Bristol, Bristol, UK.

Bouchard, P.J., George, D., Santisteban, J.R., Bruno, G., Dutta, M., Edwards, L., Kingston, E., Smith, D.J., 2005. Measurement of the residual stresses in a stainless steel pipe girth weld containing long and short repairs. International Journal of Pressure Vessels and Piping 82, 299-310.

Brown, T.B., Dauda, T.A., Truman, C.E., Smith, D.J., Memhard, D., Pfeiffer, W., 2006. Predictions and measurements of residual stress in repair welds in plates. International Journal of Pressure Vessels and Piping 83, 809-818.

Ficquet, X., Smith, D.J., Truman, C.E., Kingston, E.J., Dennis, R.J., 2009. Measurement and prediction of residual stress in a bead-on-plate weld benchmark specimen. International Journal of Pressure Vessels and Piping 86, 20-30.

Ficquet, X., Truman, C.E., Smith, D.J., Brown, B., Dauda, T., 2005. Measurement of residual stresses in large industrial components using the deep hole drilling technique, ASME Pressure Vessels and Piping Conference, Denver Colorado.

George, D., Kingston, E., Smith, D.J., 2002. Measurement of through-thickness stresses using small holes. The Journal of Strain Analysis for Engineering Design 37, 125-139.

George, D., Smith, D.J., 2005. Through thickness measurement of residual stresses in a stainless steel cylinder containing shallow and deep weld repairs. International Journal of Pressure Vessels and Piping 82, 279-287.

George, D., Smith, D.J., Bouchard, P.J., 2000. Evaluation of through wall residual stresses in stainless steel weld repairs. Materials Science Forum, 347-349, 646-651.

George, D.B.F., 2000. Determination of Residual Stress in Large Section Stainless Steel Welds, Mechanical Engineering. PhD thesis, University of Bristol, Bristol, UK.

Goudar, D.M., Kingston, E.J., Smith, M., Hossain, S., 2011. Measurement of Residual Stresses within a PWR Swaged Heater Tube. Applied Mechanics and Materials, 279-284.

Gripenberg, H., Keinanen, H., Ohms, C., Hanniner, H., Stefanescu, D., Smith, D., 2002. Prediction and measurement of residual stresses in cladded steel. Trans Tech Publications Ltd, Coimbra, Portugal, pp. 861-866.

Hilson, G., Simandjuntak, S., Flewitt, P.E.J., Hallam, K.R., Pavier, M.J., Smith, D.J., 2009. Spatial variation of residual stresses in a welded pipe for high temperature applications. International Journal of Pressure Vessels and Piping 86, 748-756.

Hossain, S., 2005. Residual stresses under conditions of high triaxiality, PhD thesis, Mechanical Engineering. PhD thesis, University of Bristol, Bristol, UK.

Hossain, S., Kingston, E., Truman, C., Smith, D., 2011. Finite element validation of the over-coring deep-hole drilling technique, The 2011 International Conference on Advances in Experimental Mechanics: Integrating Simulation and Experimentation for Validation (ISEV).

Hossain, S., Truman, C.E., Smith, D.J., 2012. Finite element validation of the deep hole drilling method for measuring residual stresses. International Journal of Pressure Vessels and Piping 93-94, 29-41.

Hossain, S., Truman, C.E., Smith, D.J., Bouchard, P.J., 2006. Measurement of Residual Stresses in a Type 316H Stainless Steel Offset Repair in a Pipe Girth Weld. Journal of Pressure Vessel Technology 128, 420-426.

Hossain, S., Truman, C.E., Smith, D.J., Ogawa, K., 2008. RESIDUAL STRESS MEASUREMENT SIMULATION IN A TYPE 316H STAINLESS STEEL GIRTH-BUTT WELD JOINT, ASME Pressure Vessels and Piping Division Conference, PVP 2008 - 61347, Chicago, Illinois, USA.

Hosseinzadeh, F., Mahmoudi, A.H., Truman, C.E., Smith, D.J., 2009a. Prediction and Measurement of Through Thickness Residual stresses in Large Quenched Components, World Congress on Engineering, London, UK.

Hosseinzadeh, F., Mahmoudi, A.H., Truman, C.E., Smith, D.J., 2010. Application of Deep Hole Drilling to the Measurement and Analysis of Residual Stresses in Steel Shrink-Fitted Assemblies. Strain 47, 412-426.

Hosseinzadeh, F., Smith, D.J., Truman, C.E., 2007a. Measured Residual Stresses in Large Steel Rolling Components, The Iron & Steel Technology Conference and Exposition (AISTech 2007), Indianapolis, USA.

Hosseinzadeh, F., Smith, D.J., Truman, C.E., 2009b. Through thickness residual stresses in large rolls and sleeves for metal working industry. Materials Science and Technology 25, 862-873.

Hosseinzadeh, F., Truman, C.E., Smith, D.J., 2007b. Measurement of residual stresses in large engineering components, 13th International Conference on Experimental Mechanics (ICEM13).

Hughes, D.J., Bruno, G., Pirling, T., Withers, P.J., 2006. Scientific Review: First Impressions of SALSA: The New Engineering Instrument at ILL. Neutron News 17, 28-32.

Hurrell, P.R., Davies, J., Leggatt, N.A., Dennis, R.J., Leggatt, R.H., 2007. Residual Stress Relaxation in a Tube Attachment Weld Inside a Pressure Vessel Forging During Post Weld Heat Treatment. ASME Conference Proceedings 2007, 873-881.

James, J., Edwards, L., 2008. Boiler Spines Residual Stress Measurements Programme Task 3.2: Esshete Ring-weld Measurements by Neutron Diffraction at the ISIS ENGIN-X Facility.

Jesensky, M., Vargova, J., 1981. Calculation and measurement of stresses in thick-walled welded pressure vessels. Savracske spravy Part 4, 79-87.

Kingston, E., Smith, D.J., 2003. Measurement of residual stresses in steel cylinders and nozzles containing repair welds, 7th International Colloquium on Asset Management of Aged Plant and Materials: Assessment Methods, pp. 185-204.

Kingston, E., Smith, D.J., Zheng, G., Gill, C., Hurrell, P., 2010. MEASUREMENT OF RESIDUAL STRESSES IN THICK SECTION STEEL ELECTRON BEAM WELDS, ASME Pressure Vessels and Piping Division Conference, Washington, USA.

Kingston, E., Stefanescu, D., Mahmoudi, A.H., Truman, C.E., Smith, D.J., 2006. Novel applicaition of the deep-hole drilling technique for measuring through-thickness residual stress distributions. Journal of ASTM International 3.

Kingston, E.J., 2003. Advances in the Deep-hole drilling technique for residual stress measurement. PhD thesis, University of Bristol, Bristol, UK.

Leggatt, N.A., Dennis, R., Hurrell, P.R., Gould, S.E., Kane, R.R., 2007. Modelling the Fabrication of a Pressure Vessel Toroidal Seal. ASME Conference Proceedings 2007, 839-849.

Leggatt, R.H., Smith, D.J., Smith, S.D., Faure, F., 1996. Development and experimental validation of the deep hole method for residual stress measurement. The Journal of Strain Analysis for Engineering Design 31, 177-186.

Mahmoudi, A., Hossain, S., Truman, C., Smith, D., Pavier, M., 2009a. A New Procedure to Measure Near Yield Residual Stresses Using the Deep Hole Drilling Technique. Experimental Mechanics 49, 595-604.

Mahmoudi, A.H., Moud, S.H., Truman, C.E., Smith, D.J., 2003. Measurement and Prediction of Residual Stress Generated by Local Compression, European Solid Mechanics Conference-ESMC5.

Mahmoudi, A.H., Pavier, M.J., Truman, C.E., Smith, D.J., 2007. Accurate measurement of highly triaxial residual stresses, The Society of Experimental Mechanics (SEM), Springfield, USA.

Mahmoudi, A.H., Smith, D.J., Truman, C.E., Pavier, M.J., 2009c. APPLICATION OF THE MODIFIED DEEP HOLE DRILLING TECHNIQUE (iDHD) FOR MEASURING NEAR YIELD NON-AXISYMMETRIC RESIDUAL STRESSES, in: PVP2009-77940 (Ed.), ASME Pressure Vessels and Piping Division Conference, Prague, Czech Republic, pp. PVP2009-77940.

Mahmoudi, A.H., Stefanescu, D., Hossain, S., Truman, C.E., Smith, D.J., Withers, P.J., 2006. Measurement and prediction of the residual stress field generated by side-punching. Journal of Engineering Materials and Technology 128, 451-459.

Mahmoudi, A.H., Truman, C.E., Smith, D.J., Pavier, M.J., 2011. The effect of plasticity on the ability of the deep hole drilling technique to measure axisymmetric residual stress. International Journal of Mechanical Sciences 53, 978-988.

Mirzaee-Sisan, A., Fookes, A.J., Truman, C.E., Smith, D.J., Brown, T.B., Dauda, T.A., 2007. Residual stress measurement in a repair welded header in the as-welded condition and after advanced post weld treatment. International Journal of Pressure Vessels and Piping 84, 265-273.

Ohms, C., Truman, C., Wimpory, R.C., Gripenberg, H., Smith, D., Youtsos, A.G., 2006. Measurement of residual stress in as received and repaired clad components, Pressure Vessels and Piping Division (Publication) PVP. American Society of Mechanical Engineers, Vancouver, BC, Canada.

Pirling, T., Bruno, G., Withers, P.J., 2006a. SALSA-A new instrument for strain imaging in engineering materials and components. Materials Science and Engineering: A 437, 139-144.

Pirling, T., Bruno, G., Withers, P.J., 2006b. SALSA - A new instrument for strain imaging in engineering materials and components. Materials Science and Engineering: A 437, 139-144.

Poussard, C., Pavier, M.J., Smith, D.J., 1995. Analytical and finite element predictions of residual stresses in cold worked fastener holes. The Journal of Strain Analysis for Engineering Design 30, 291-304.

R6-Revision4, 2009. Assessment of the integrity of structures containing defects, Section III.15, Gloucester, UK: British Energy Generation Ltd, Amendment 7.

Robinson, J.S., Hossain, S., Truman, C.E., Paradowska, A.M., Hughes, D.J., Wimpory, R.C., Fox, M.E., 2010. Residual stress in 7449 aluminium alloy forgings. Materials Science and Engineering: A 527, 2603-2612.

Robinson, J.S., Truman, C.E., Hossain, S., Wimpory, R., 2008. Residual stress and microstructural variations in thick aluminium alloy forgings. Materials Science Forum 571-572, 45-50.

Smith, D.J., Bouchard, P.J., George, D., 2000. Measurement and prediction of residual stresses in thick-section steel welds. The Journal of Strain Analysis for Engineering Design 35, 287-305.

Stefanescu, D., Truman, C.E., Smith, D.J., 2004. An integrated approach for measuring near-surface and subsurface residual stress in engineering components. The Journal of Strain Analysis for Engineering Design 39, 483-497.

TWI-Report, April 2005. Manufacture of Esshete Ring-weld Test Specimen, p. Report No. 15708/15701/15705.

Wang, S., Li, Y., Yao, M., Wang, R., 1998. Compressive residual stress introduced by shot peening. Journal of Materials Processing Technology 73, 64-73.

Wimpory, R., Stefanescu, D., Smith, D.J., O'Dowd, N.P., Webster, G.A., May, P.S., Kingston, E., 2003a. Residual stress distributions in welded ferritic steel T-plate joints, MECA-Sens: Stress Evaluation by Neutron and Synchrotron Radiation.

Wimpory, R.C., May, P.S., O'Dowd, N.P., Webster, G.A., Smith, D.J., Kingston, E., 2003b. Measurement of residual stresses in T-plate weldments. The Journal of Strain Analysis for Engineering Design 38, 349-365.

Yaghi, A.H., Hyde, T.H., Backer, A.A., Sun, W., Hilson, G., Simandjuntak, S., Flewitt, P.E.J., Pavier, M.J., Smith, D.J., 2010. A Comparison Between Measured and Modeled Residual Stresses in a Circumferentially Butt-Welded

P91 Steel Pipe. JOURNAL OF PRESSURE VESSEL TECHNOLOGY-TRANSACTIONS OF THE ASME, 132.

Zhdanov, I.M., Gonchar, A.K., 1978. Determining the residual welding stresses at a depth in metals. Automatic Welding 31, 22-24.

Zheng, G., 2013. Development of the deep-hole drilling method for residual stress measurement in metallic welds. PhD thsis, Univeristy of Bristol, Bristol, UK.

Table 1 Material properties of Esshette 1250 weld and parent stainless steel (Wang et al., 1998)

Temp.	Density	Conductivity	Specific Heat	Film property	Thermal Expansion	Parent Young's Modulus	weld Young's Modulus	Posson's Ratio
ºC	Kg/m3	W/m*K	J/Kg*K	W/m2*K	m/m*K	Pa	Pa	
20	7960	12.69	490	4.15	1.54E-05	2.05E+11	1.72E+11	0.294
100	7930	13.93	508	5.03	1.60E-05	1.97E+11	1.65E+11	0.294
200	7890	15.48	532	5.99	1.67E-05	1.88E+11	1.57E+11	0.294
300	7850	17.03	555	6.70	1.73E-05	1.80E+11	1.50E+11	0.294
400	7810	18.58	580	7.46	1.79E-05	1.73E+11	1.43E+11	0.294
500	7770	20.13	603	8.22	1.84E-05	1.65E+11	1.36E+11	0.294
600	7730	21.68	627	9.06	1.89E-05	1.56E+11	1.28E+11	0.294
700	7680	23.23	650	9.78	1.94E-05	1.46E+11	1.19E+11	0.294
800	7640	24.78	650	10.53	1.98E-05	1.35E+11	1.09E+11	0.294
900	7600	26.33	650	11.33	2.02E-05	1.21E+11	9.77E+10	0.294
1000	7550	27.88	650	11.77	2.05E-05	1.04E+11	8.41E+10	0.294
1100	7550	29.43	650	12.21	2.08E-05	8.48E+10	6.80E+10	0.294
1200	7550	30.98	650	12.57	2.10E-05	6.15E+10	4.92E+10	0.294
1300	7550	32.53	650	12.89	2.12E-05	3.41E+10	2.72E+10	0.294
1400	7550	34.08	650	13.21	2.14E-05	2.00E+09	1.70E+09	0.294

Table 2 True stress-strain data of Esshette 1250 weld and parent stainless steel (Wang et al., 1998)

	Parent						Weld	
Temp.	0% Plastic Strain	0.2% Plastic Strain	1% Plastic Strain	1.98% Plastic Strain	4.88% Plastic Strain	10% Plastic Strain	0% Plastic Strain	10% Plastic Strain
ºC	Pa	Pa	Pa	Pa	Pa	Pa	Pa	Pa
20	3.08E+08	3.24E+08	3.87E+08	4.16E+08	4.75E+08	5.29E+08	5.29E+08	5.32E+08
250	2.28E+08	2.41E+08	2.90E+08	3.16E+08	3.75E+08	4.70E+08	4.70E+08	4.72E+08
500	1.93E+08	2.04E+08	2.51E+08	2.76E+08	3.43E+08	4.15E+08	4.15E+08	4.17E+08
600	1.94E+08	2.05E+08	2.50E+08	2.77E+08	3.40E+08	3.82E+08	3.82E+08	3.84E+08
750	1.64E+08	1.70E+08	1.95E+08	2.10E+08	2.34E+08	2.51E+08	3.05E+08	3.07E+08
900	8.70E+07					8.74E+07	1.59E+08	1.60E+08
1100	3.80E+07					3.82E+07	5.30E+07	5.33E+07
1400	3.80E+06					3.80E+06	5.30E+06	5.30E+06

Table 3 Welding input data for 7 passes

Pass	Heat Input	Advance Rate	Area	Pass Length	Body Flux*	weld efficiency	Reduced Body Flux
	J/m	m/s	m2	m	J/s*m3		J/s*m3
1	1.58	2.60E-03	2.72E-05	0.251	6.01E+08	0.60	3.61E+08
2	2.12	1.90E-03	3.65E-05	0.251	4.39E+08	0.75	3.29E+08
3	2.93	1.40E-03	5.05E-05	0.251	3.23E+08	0.75	2.42E+08
4	1.63	2.50E-03	2.81E-05	0.230	6.31E+08	0.70	4.42E+08
5	1.59	2.50E-03	2.74E-05	0.273	5.32E+08	0.75	3.99E+08
6	1.96	2.30E-03	3.38E-05	0.227	5.87E+08	0.70	4.11E+08
7	1.84	2.60E-03	3.17E-05	0.276	5.48E+08	0.75	4.11E+08

* Body flux was calculated by (Heat Input) ×(Advance Rate)/ (Area ×Pass Length)

Table 4 Summary of different deep-hole drilling process simulations undertaken

	Standard DHD	iDHD	oDHD	Start Location		Drill		Trepan	
				Top	Bottom	Plastic	Elastic	Plastic	Elastic
DH1	✓				✓	✓		✓	
DH2		✓			✓	✓		✓	
DH3			✓		✓	✓		✓	

Table 5 Standard DHD parametric study

	Standard DHD	iDHD	Start Location		Drill		Trepan	
			Weld Top	Parent Bottom	Plastic	Elastic	Plastic	Elastic
DH1	✓			✓	✓		✓	
DH4	✓		✓		✓		✓	
DH5	✓		✓		✓			✓
DH6	✓		✓			✓		✓

Table 6 Over-coring DHD (oDHD) parametric study

	oDHD	Drill- Plastic	Trepan 1		Trepan 2	Trepan 3	Trepan 4
		Ø1.5	Ø40	Ø17	Ø17	Ø12	Ø5
DH3	✓	✓	✓				✓
DH7	✓	✓	✓		✓		✓
DH8	✓	✓				✓	✓
DH9	✓	✓		✓			✓

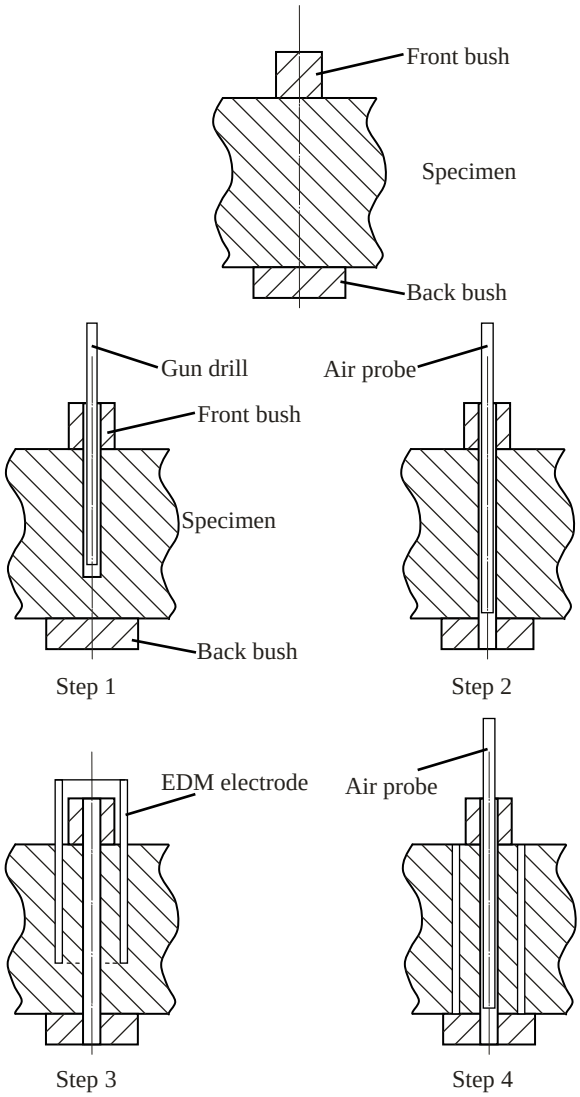

Figure 1 Schematic illustration of the procedures in standard DHD technique: step 1: drilling a reference hole; step 2: measurement of reference hole diameter; step 3: core trepanning and step 4: re-measurement of hole diameter

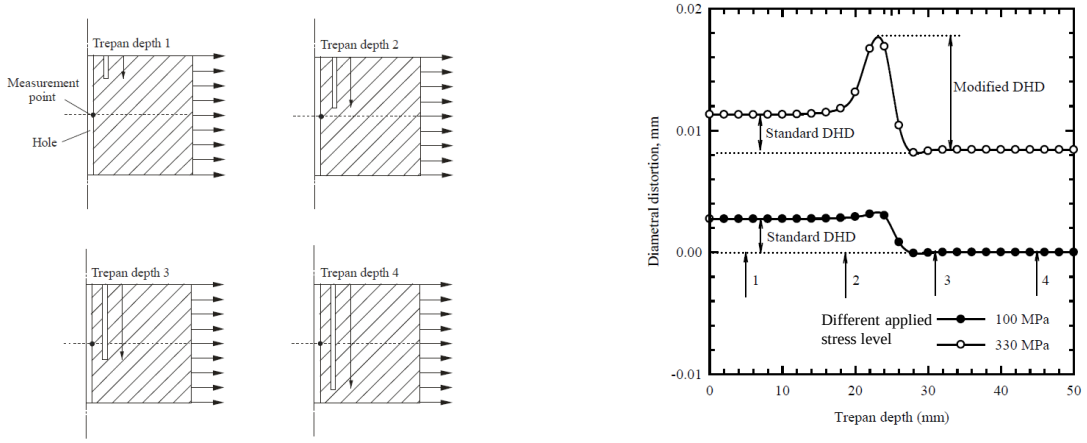

Figure 2 Comparison of hole distortions for two different levels of applied stress: (a) position of measurement and (b) diametral distortion versus trepan depth

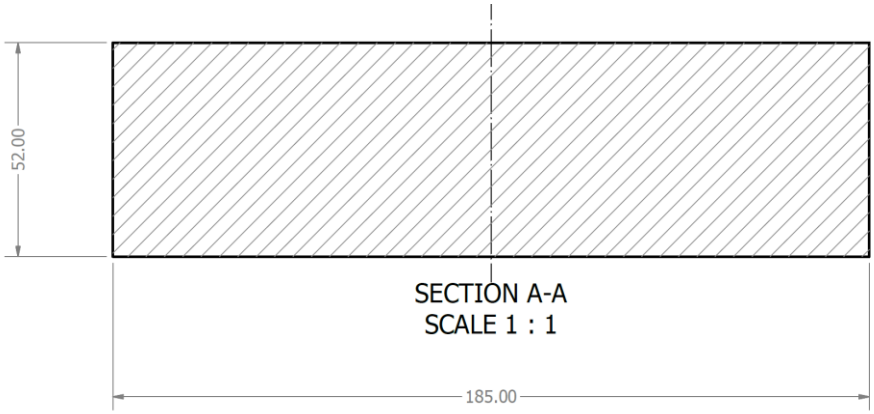

(a) Quenching

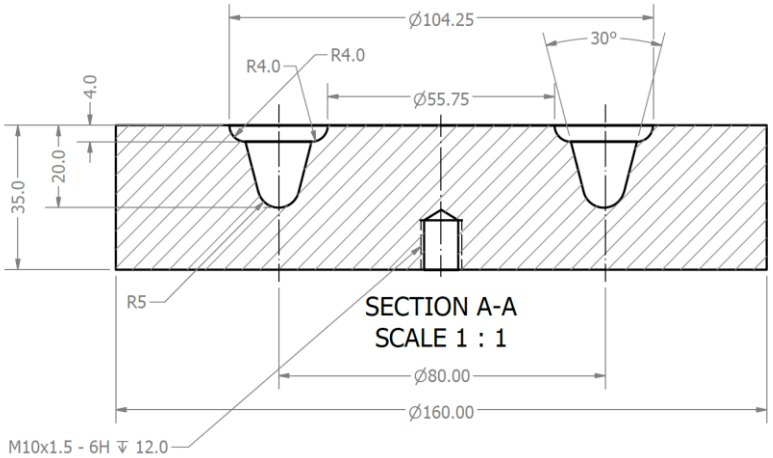

(b) Machine after quenching

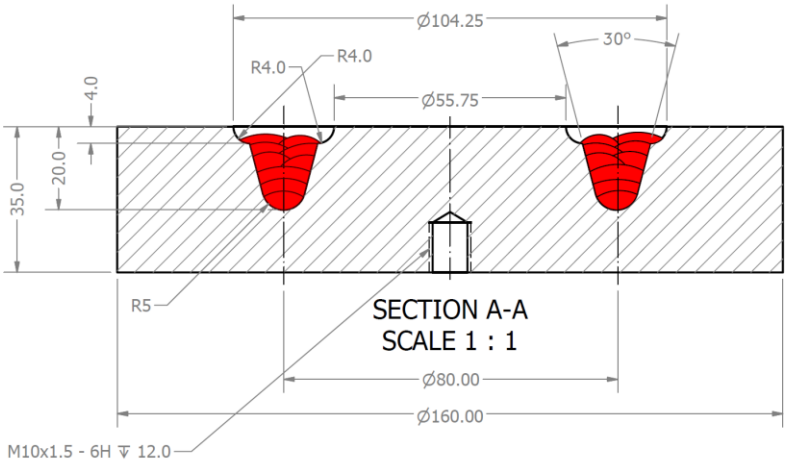

(c) Welding

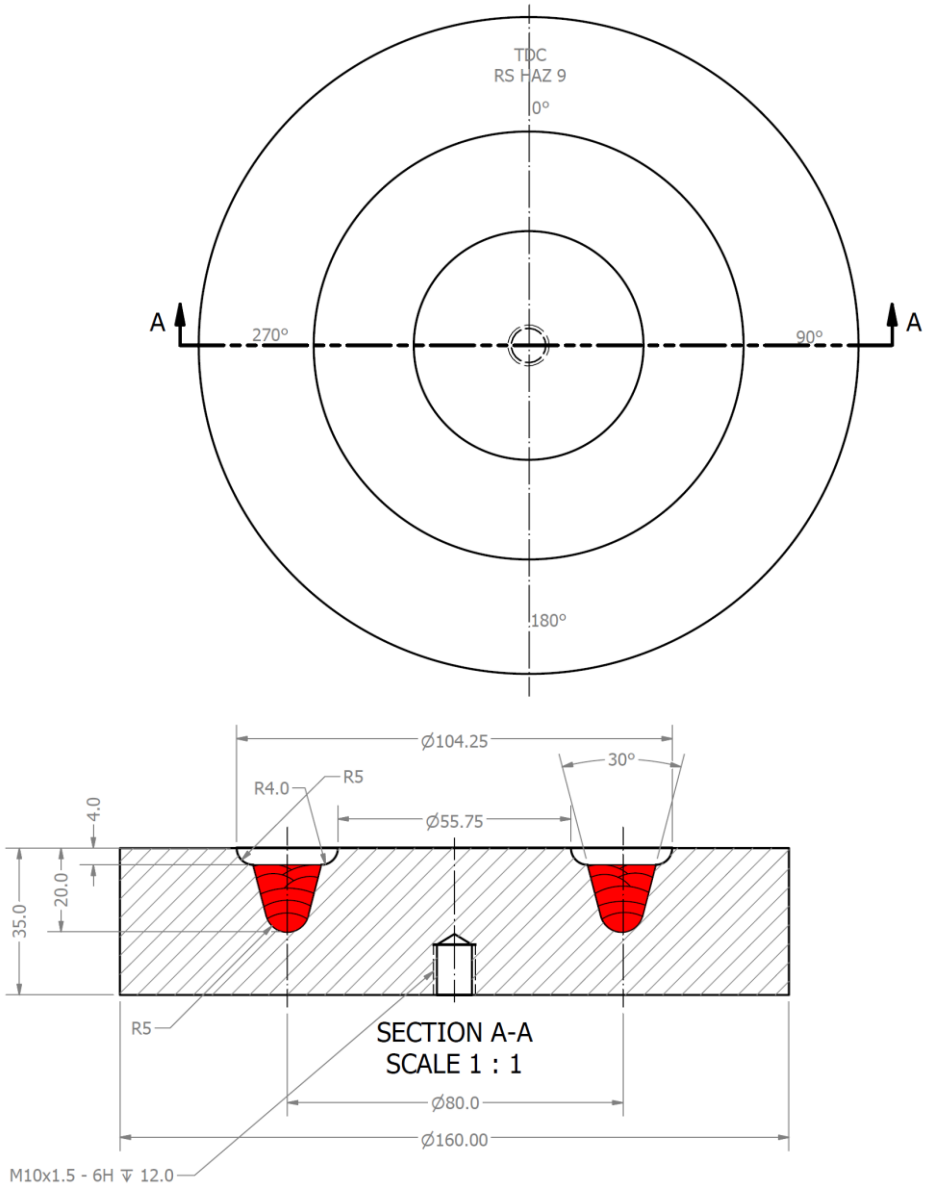

(d) Final machine after welding

Figure 3 Specimen life cycle

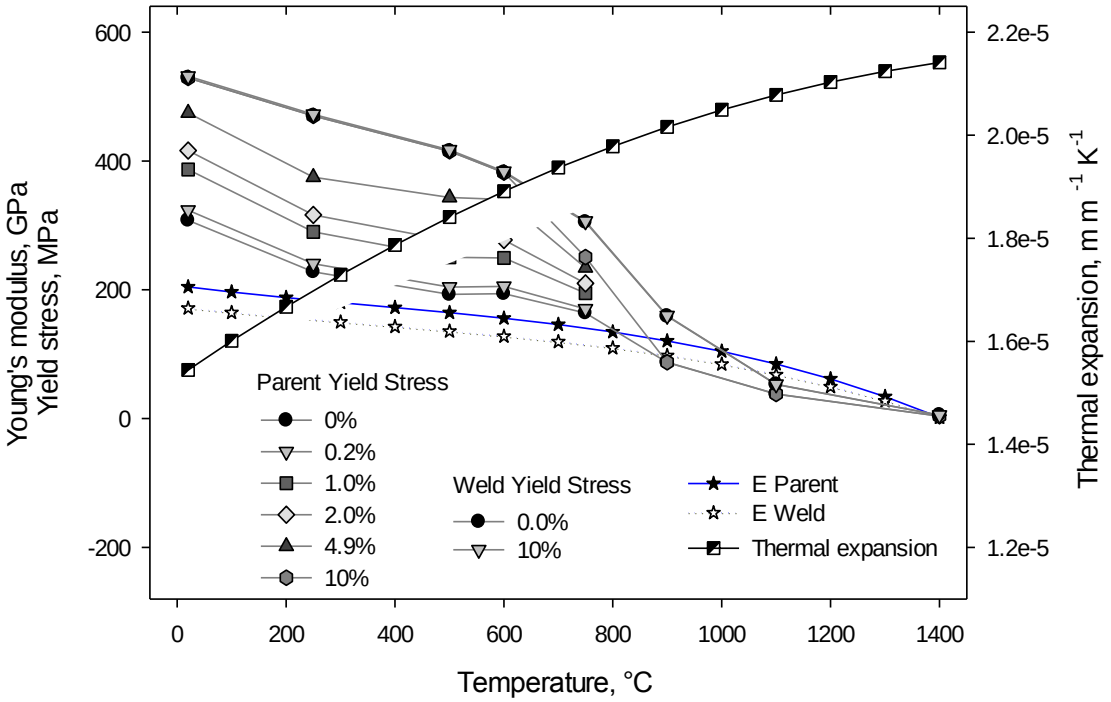

Figure 4 Esshete 1250 stainless steel mechanical properties

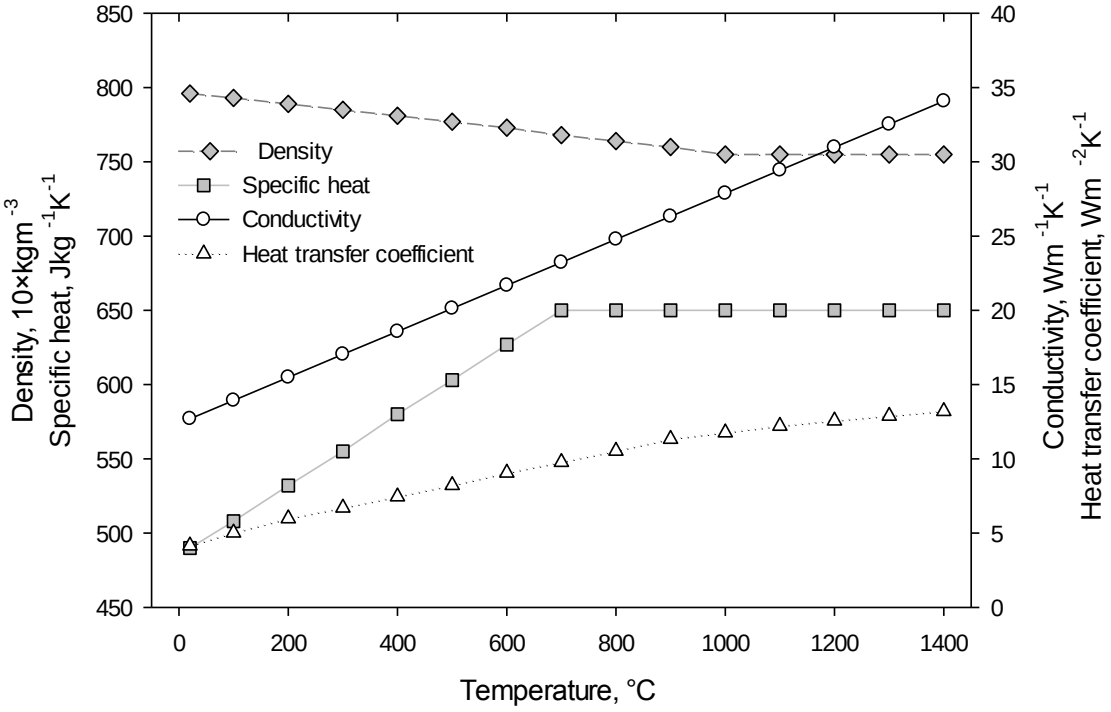

Figure 5 Esshete 1250 stainless steel physical properties

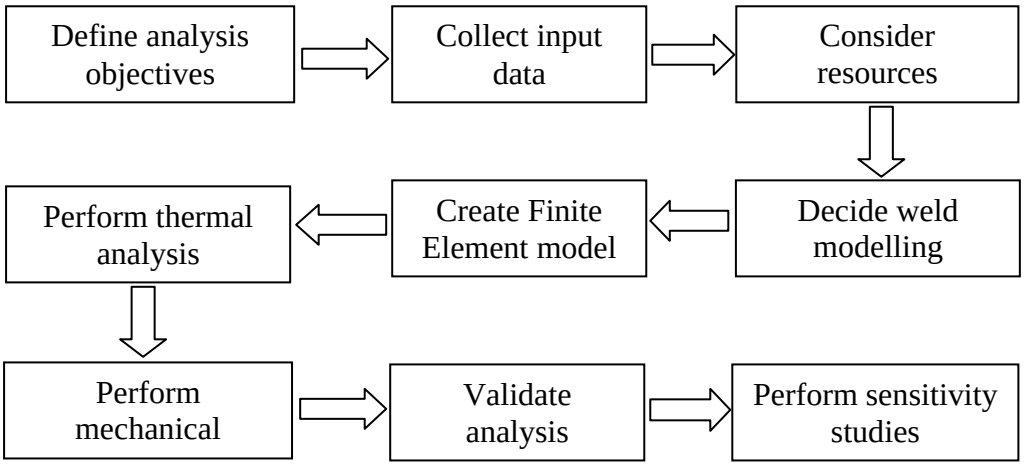

Figure 6 R6 standard flowchart for weld modelling simulation

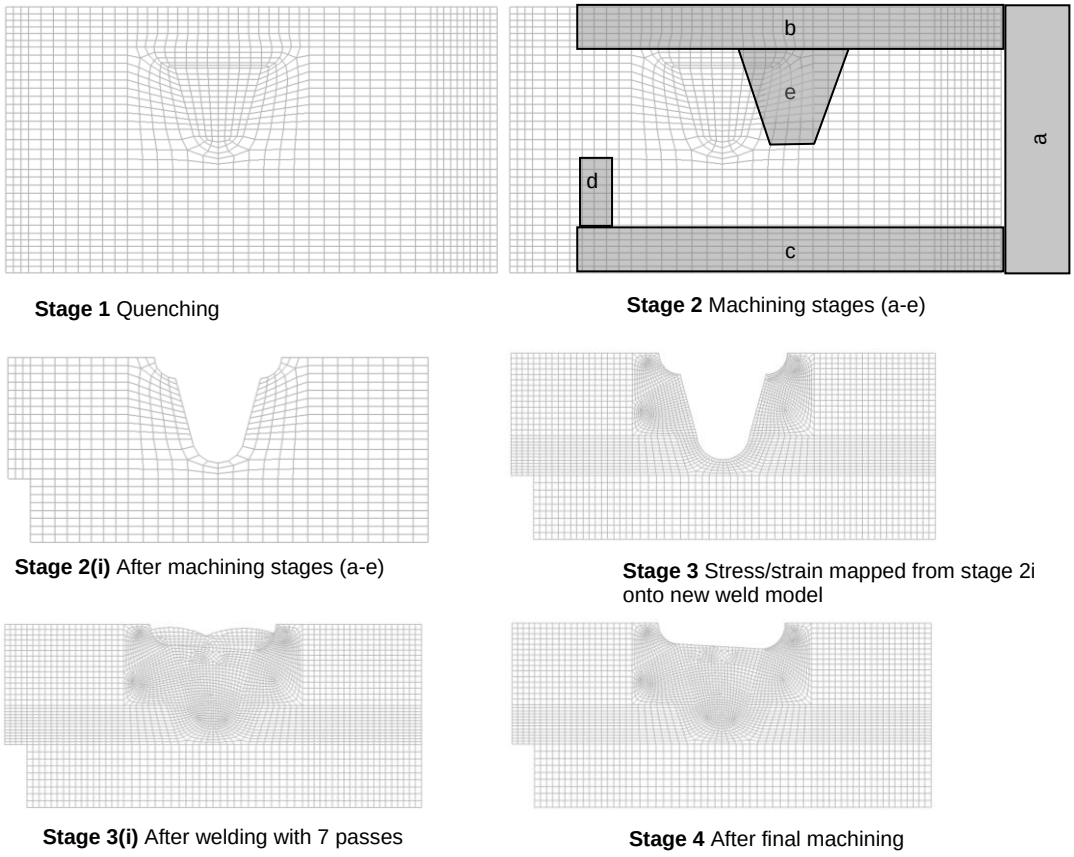

Figure 7 FEA modelling procedures for quench/weld and mapping (all in 2D axisymmetric)

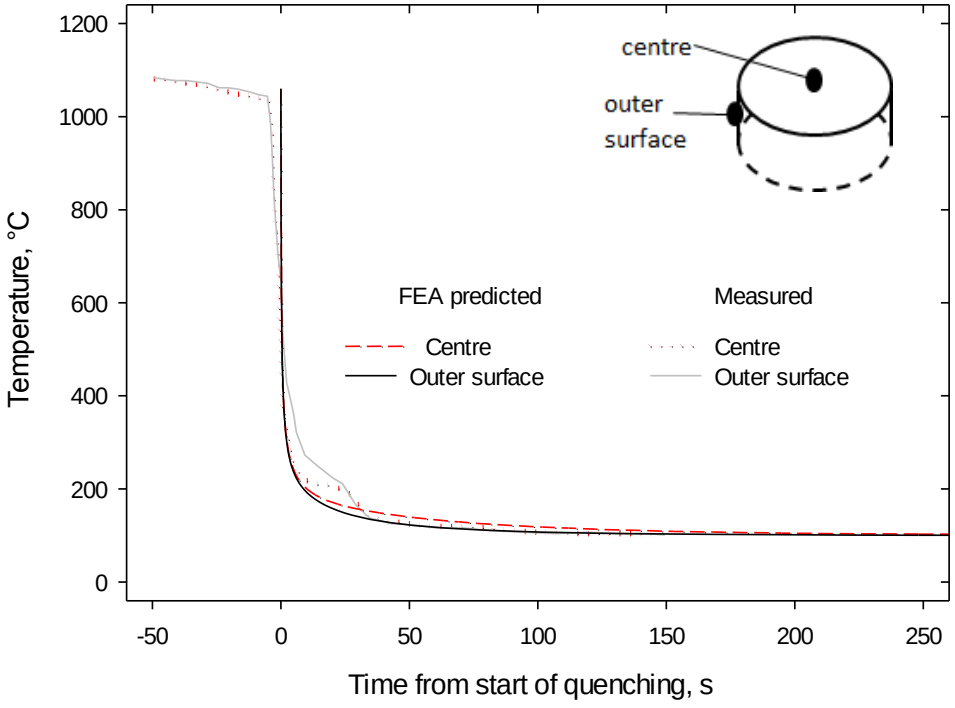

Figure 8 Comparison between the simulated and the measured temperature-time history during quenching

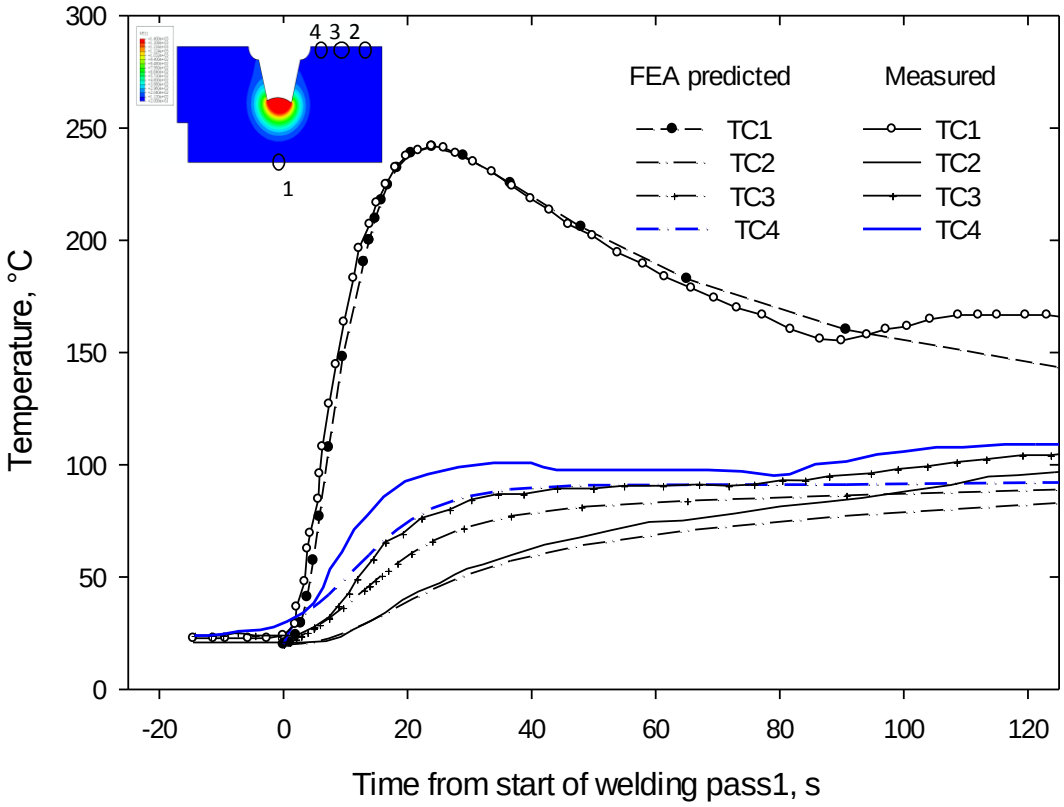

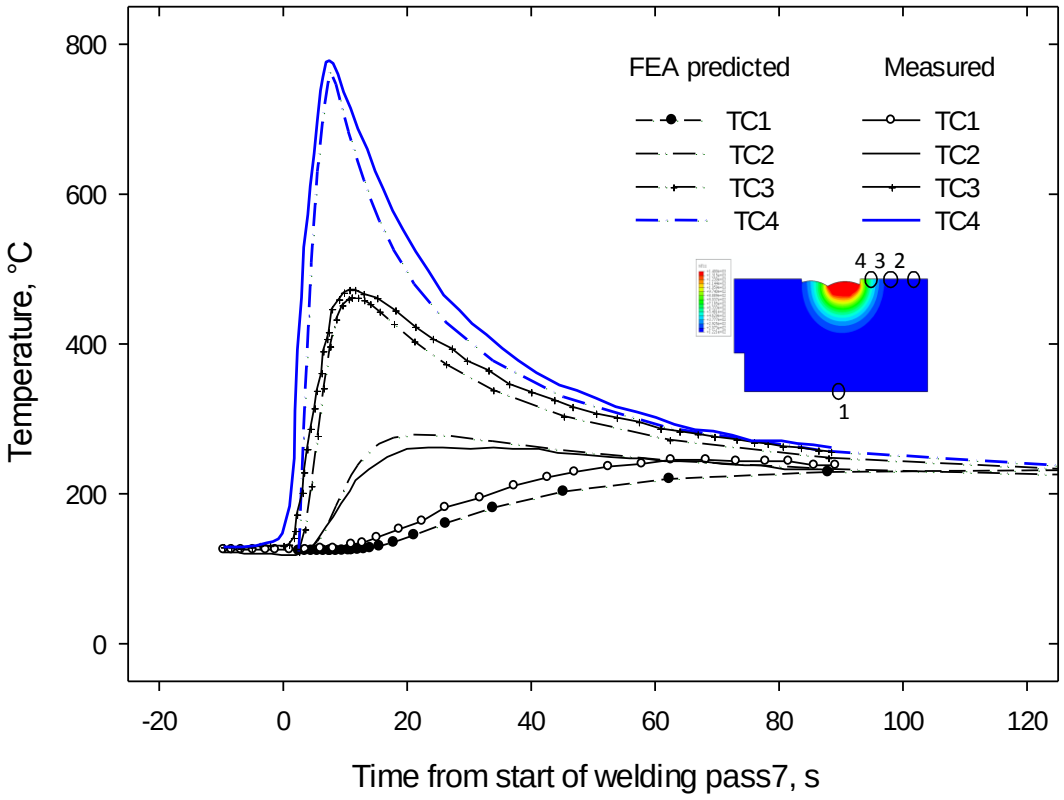

Figure 9 Comparison of simulated temperature-time history with measured during welding (for selected weld passes)

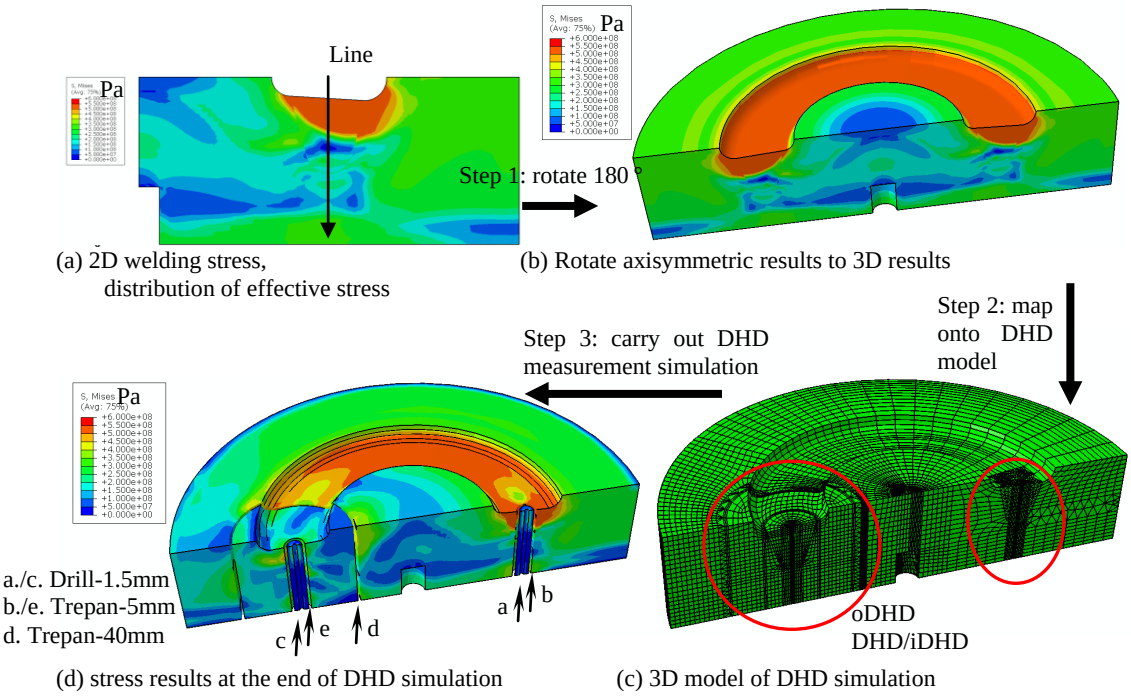

Figure 10 Main steps in deep-hole drilling simulation

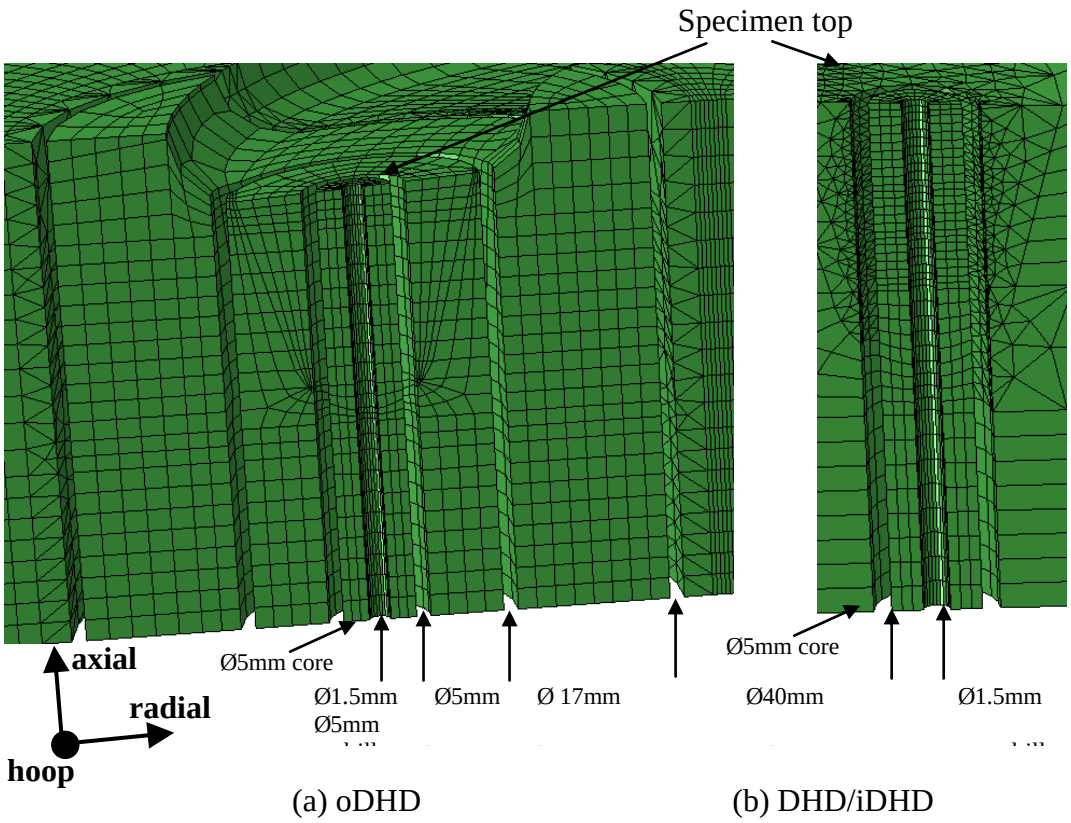

Figure 11 Details of the mesh for the deep-hole drilling simulation in the 3D model

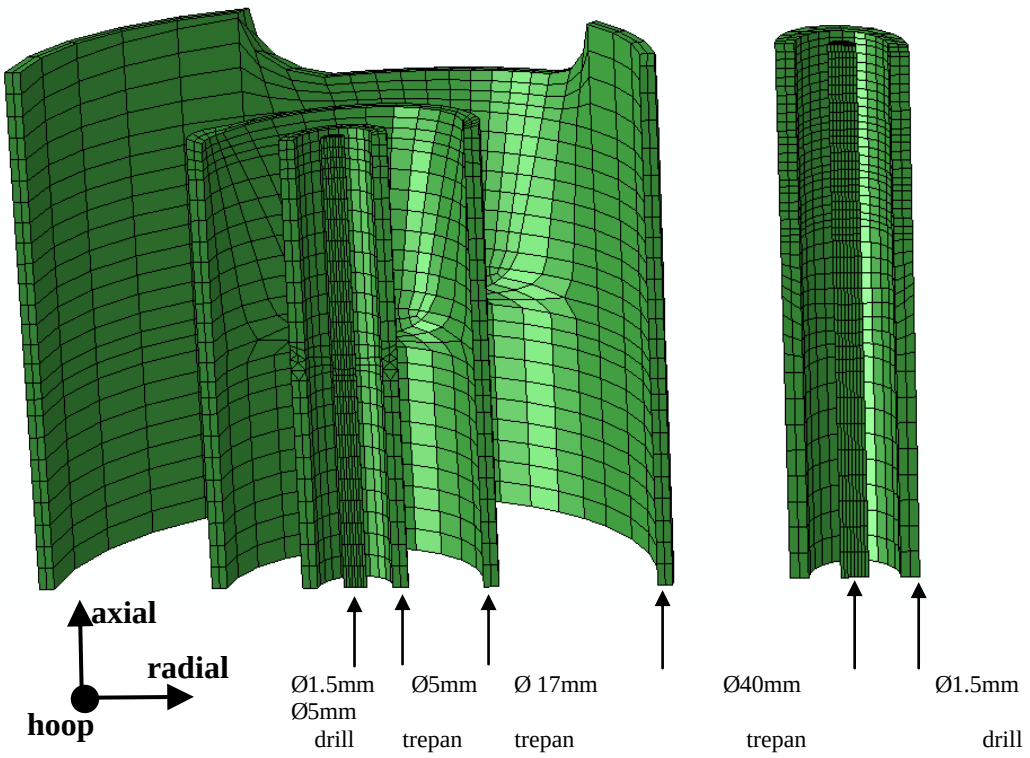

(a) oDHD (b) DHD/iDHD

Figure 12 Illustration of drill and trepan parts

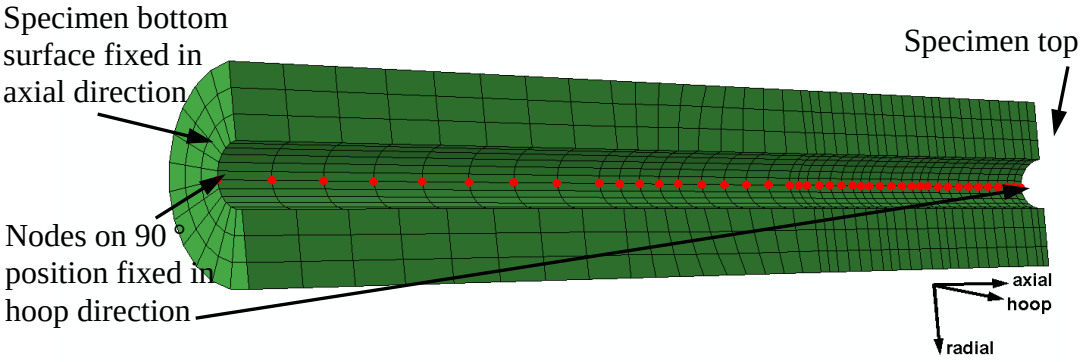

Figure 13 Boundary conditions on the Ø5mm core (1) Nodes on the 90 ° position fixed in radial direction. (2) Back bush fixed in the axial direction during the deep-hole drilling simulation

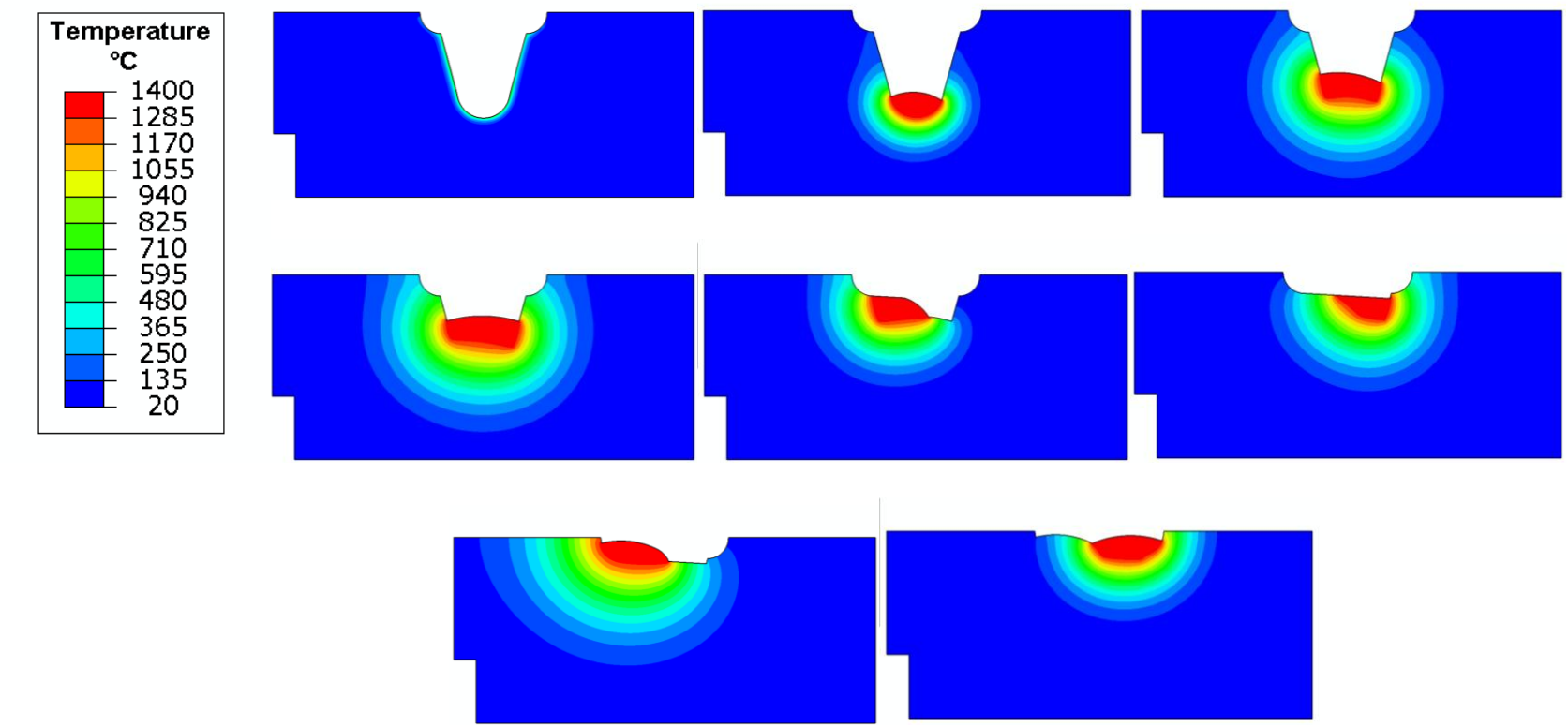

Figure 14 Predicted fusion boundaries for each pass, ℃

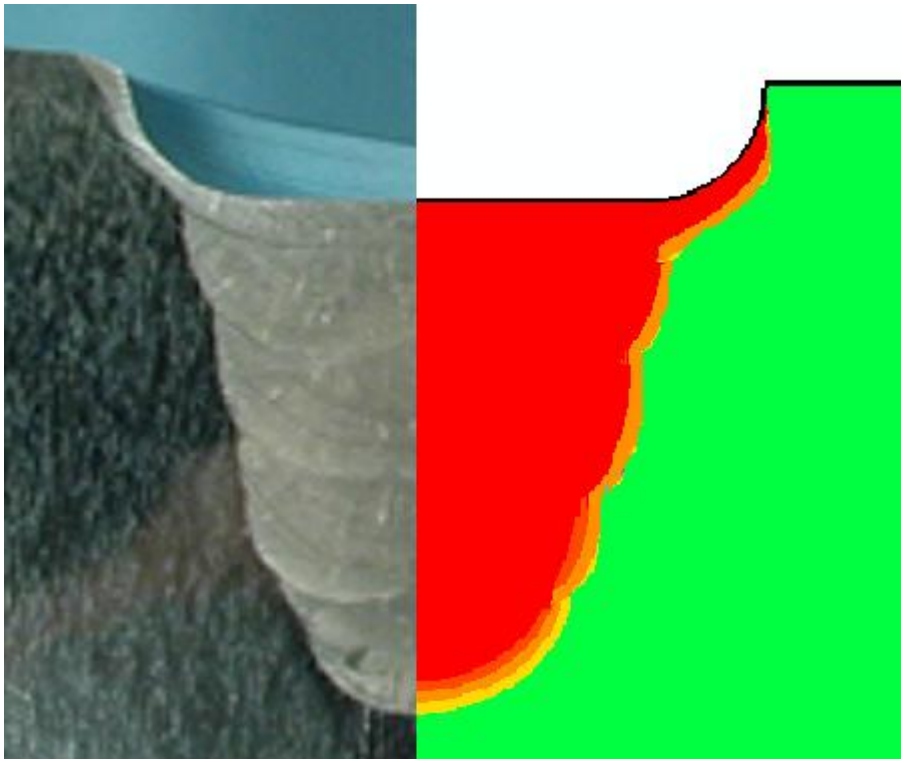

Figure 15 Macrograph compared with FEA fusion boundary

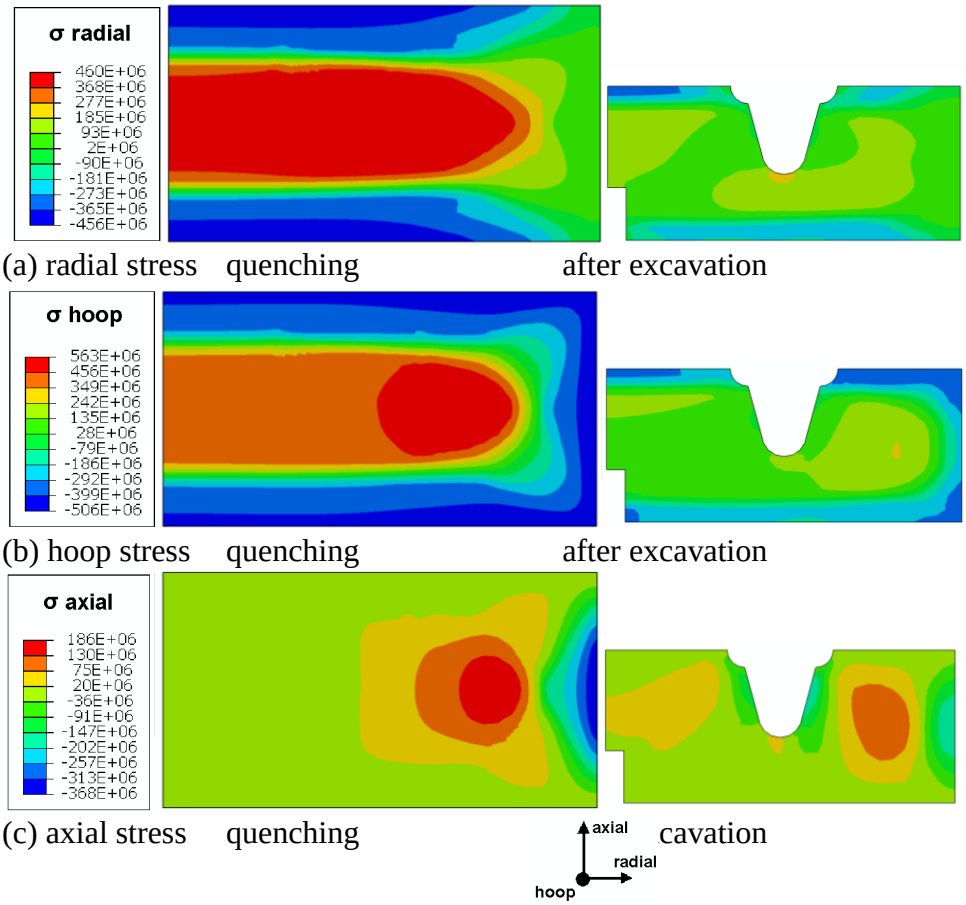

Figure 16 Residual stress contour plots from quenching and excavation

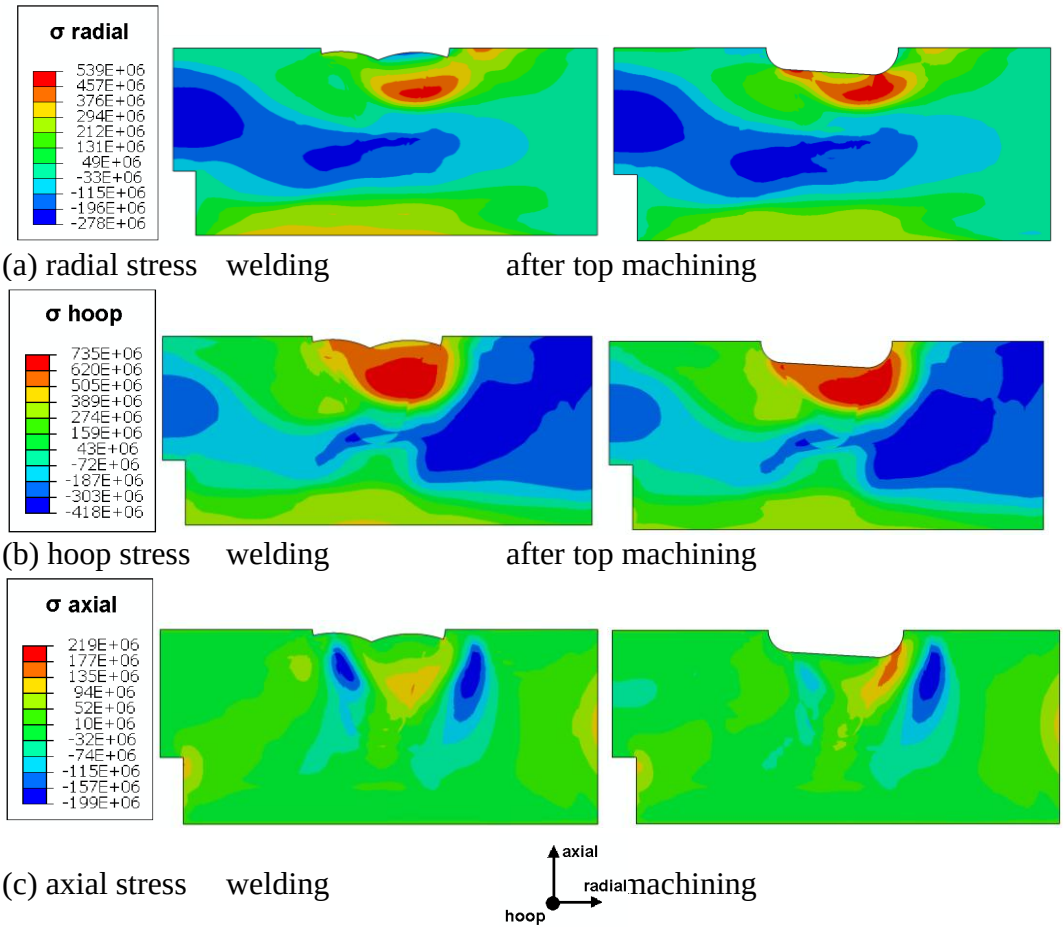

Figure 17 Contour plots showing residual stress fields generated (a) during quenching and (b) welding

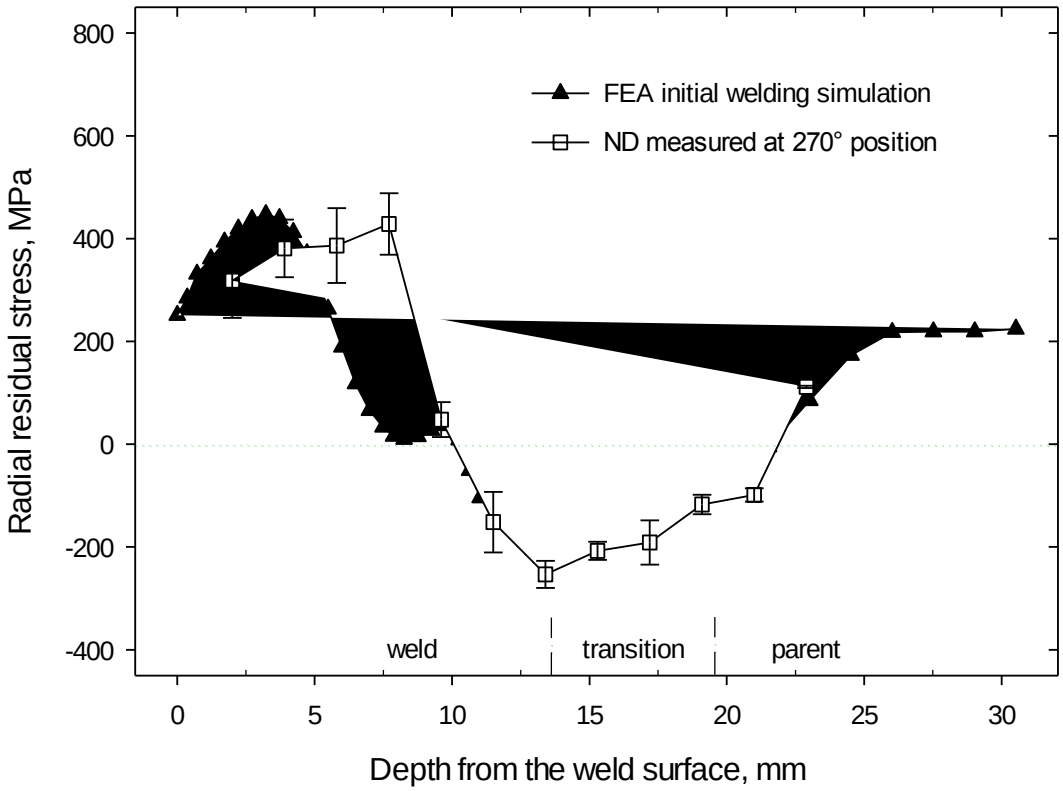

(a) Radial residual stress

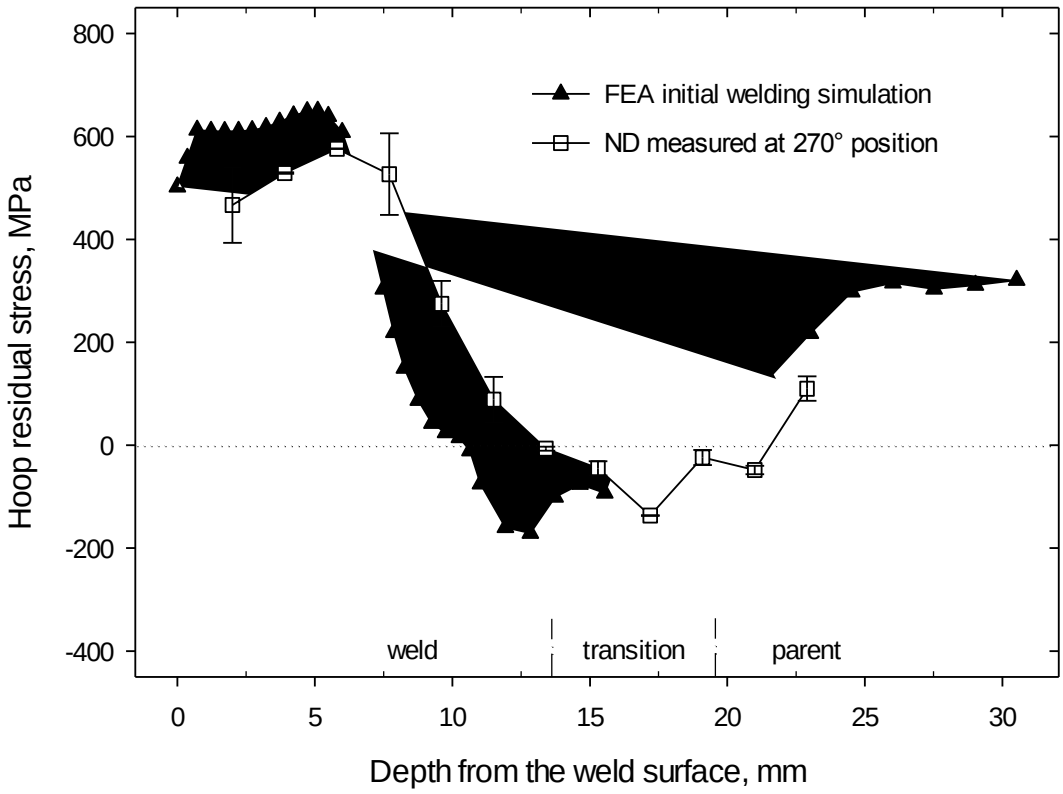

(b) Hoop residual stress

Figure 18 Comparison of measured residual stresses by the ND technique at 270 ° position with the welding simulation

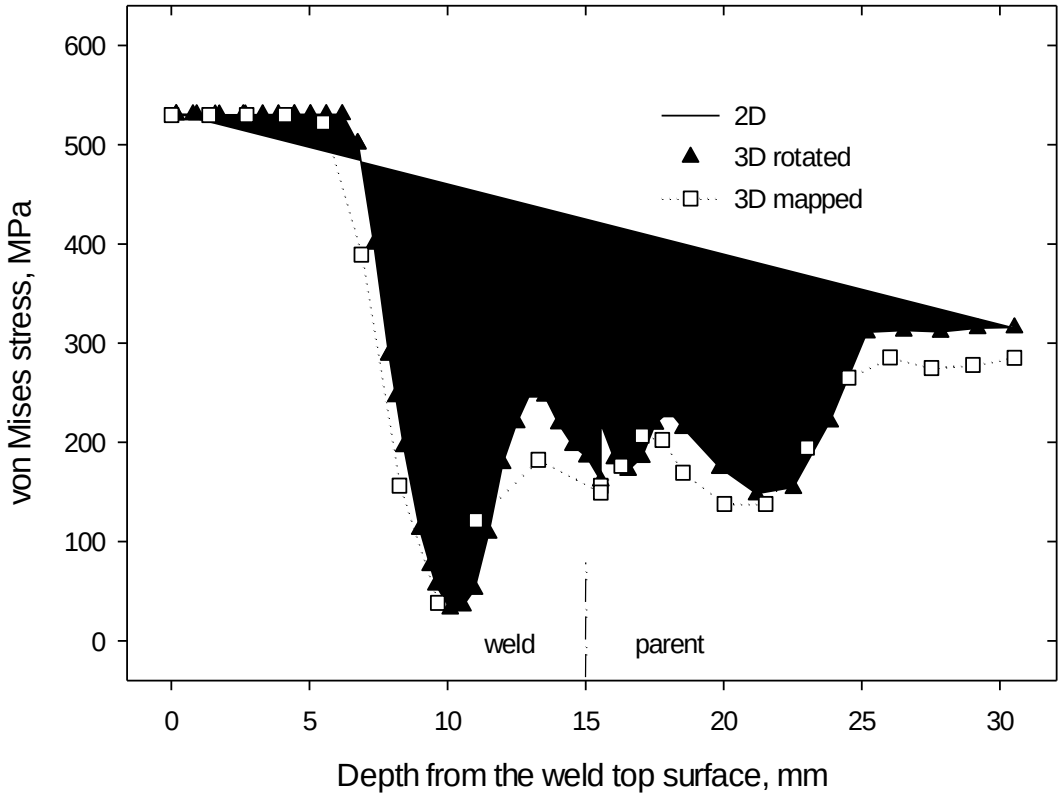

(a) Effective stress

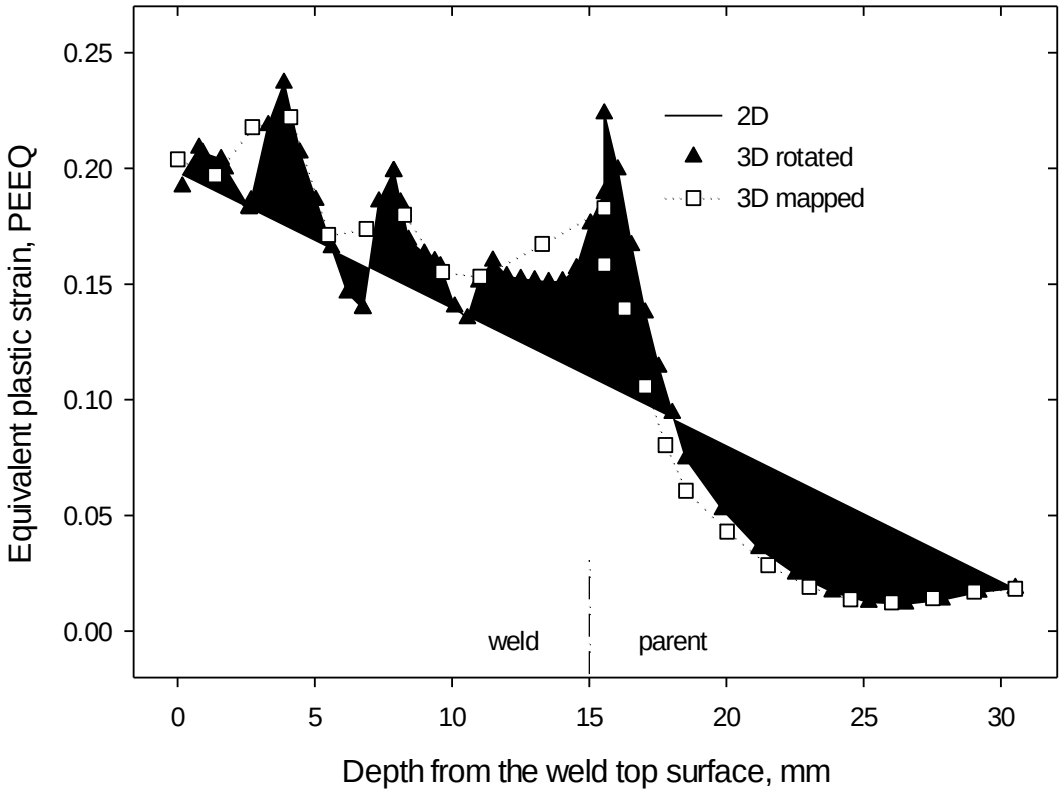

(b) PEEQ

Figure 19 Comparison of results along the centre of the groove weld (a) 2D axisymmetric, (b) 3D rotated and (c) 3D mapped results

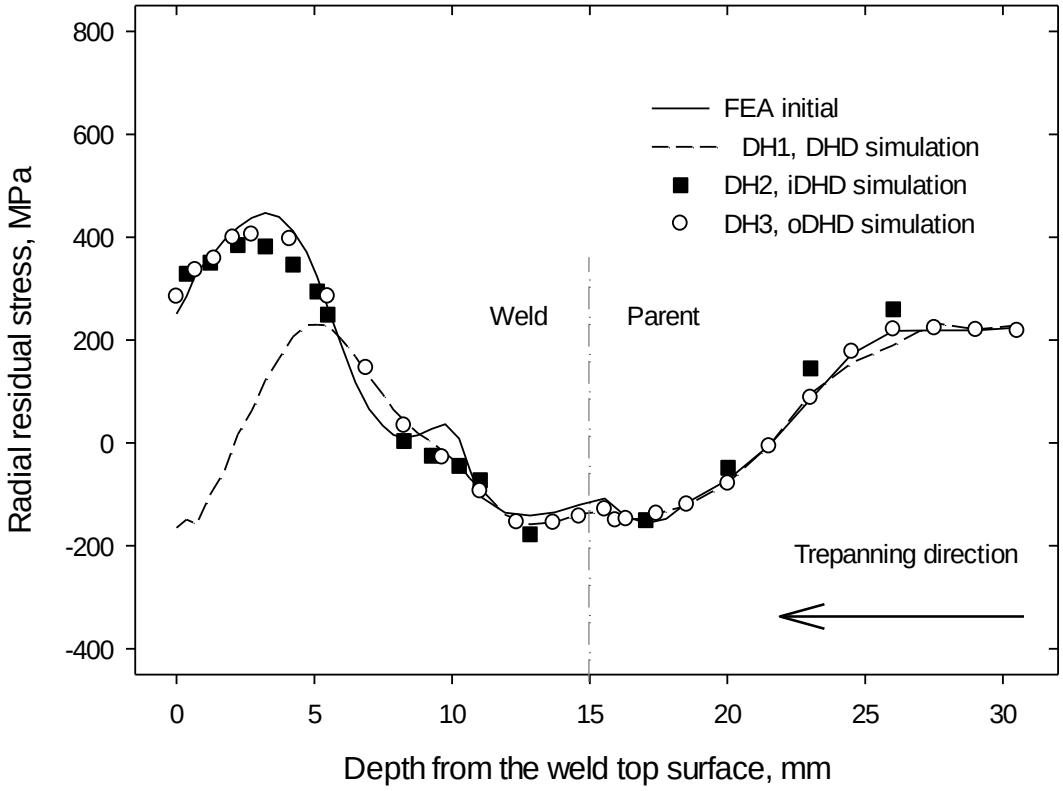

(a) Radial stress

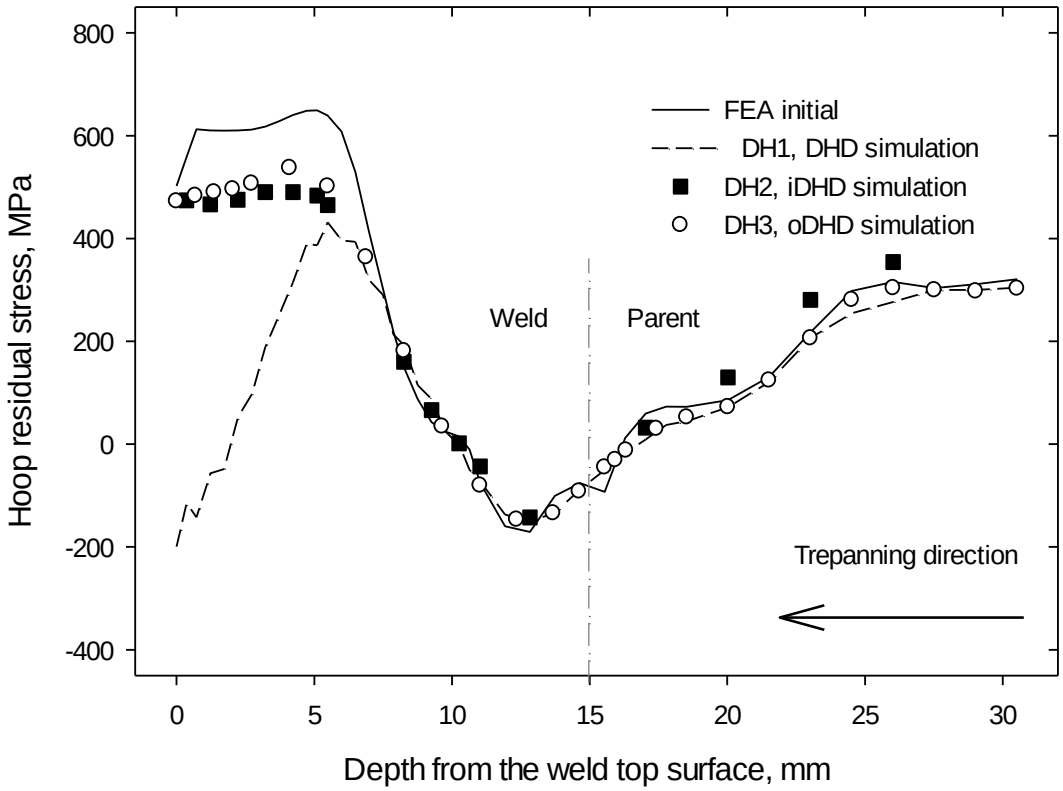

(b) Hoop stress

Figure 20 Comparison of initial residual stress distributions with standard DHD (DH1), iDHD (DH2) and oDHD (DH3) measurement simulations

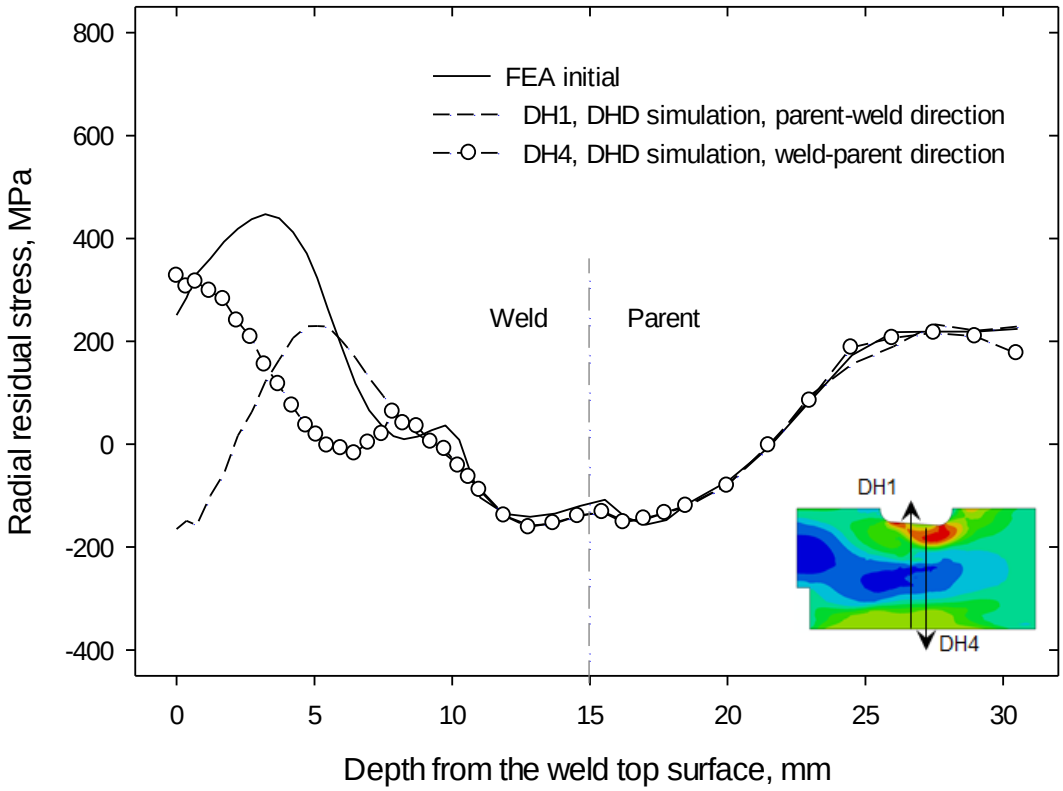

(a) Radial stress

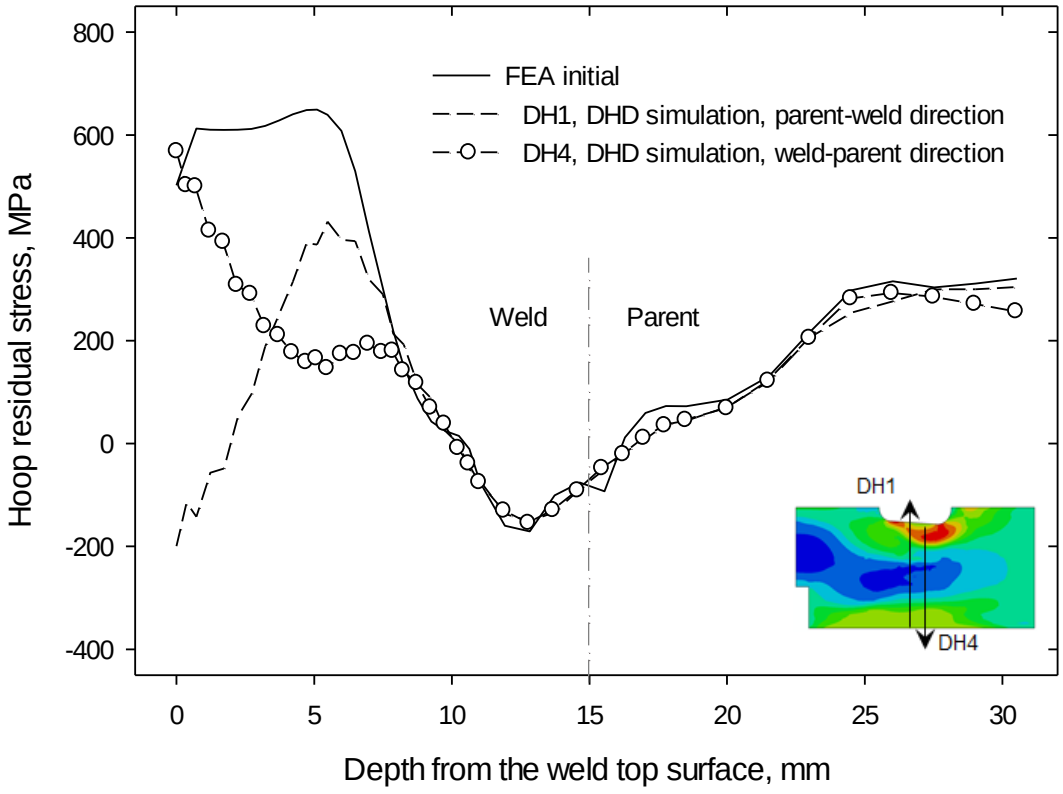

(b) Hoop stress

Figure 21 Standard DHD simulation parametric study, influence of trepan direction

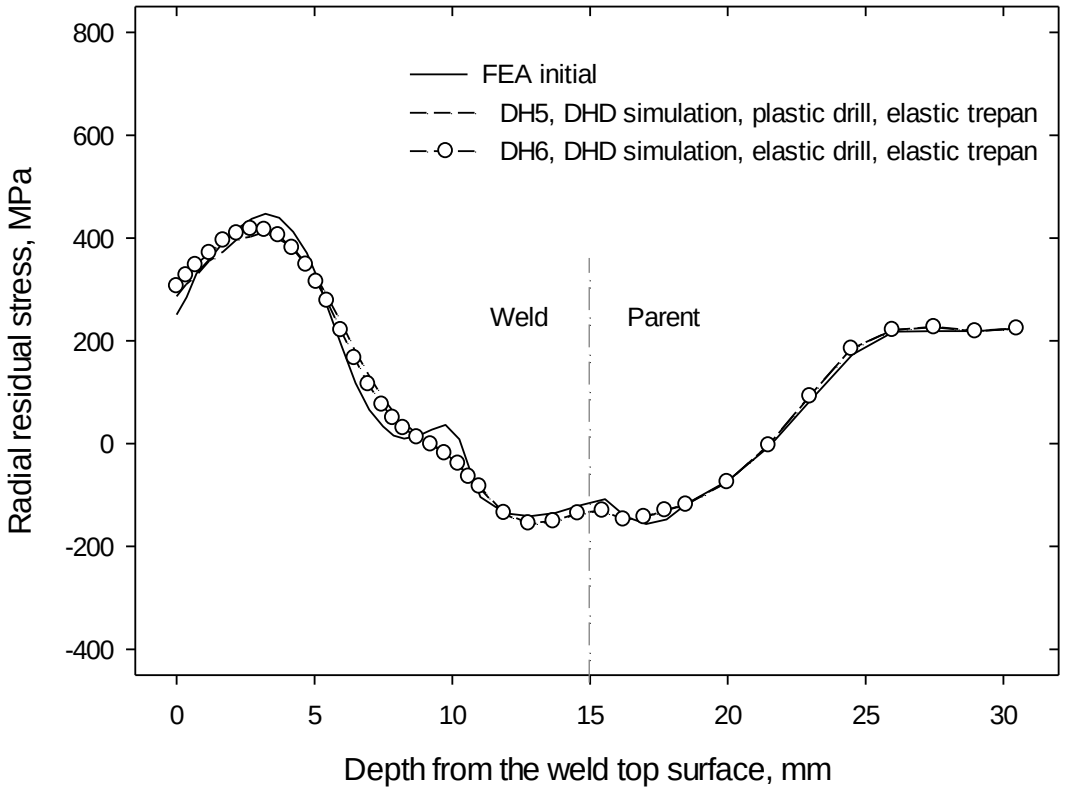

(a) Radial stress

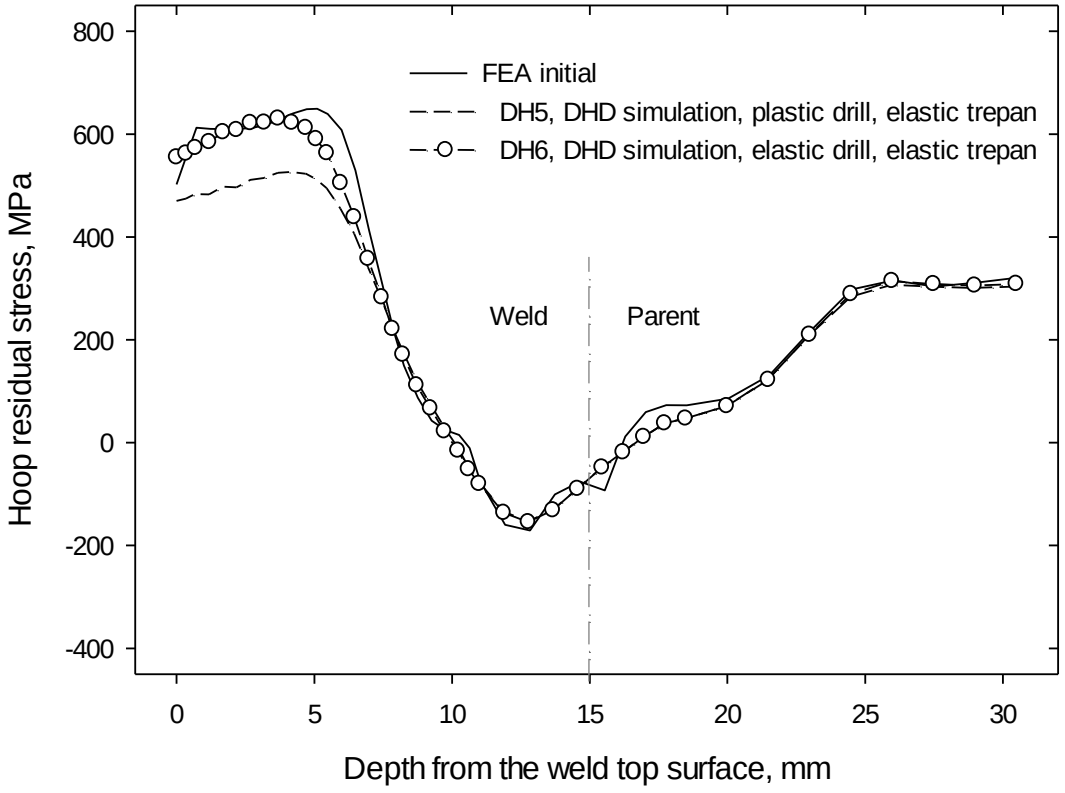

(b) Hoop stress

Figure 22 Standard DHD simulation parametric study, influence of drill and trepan produces on the initial stress field

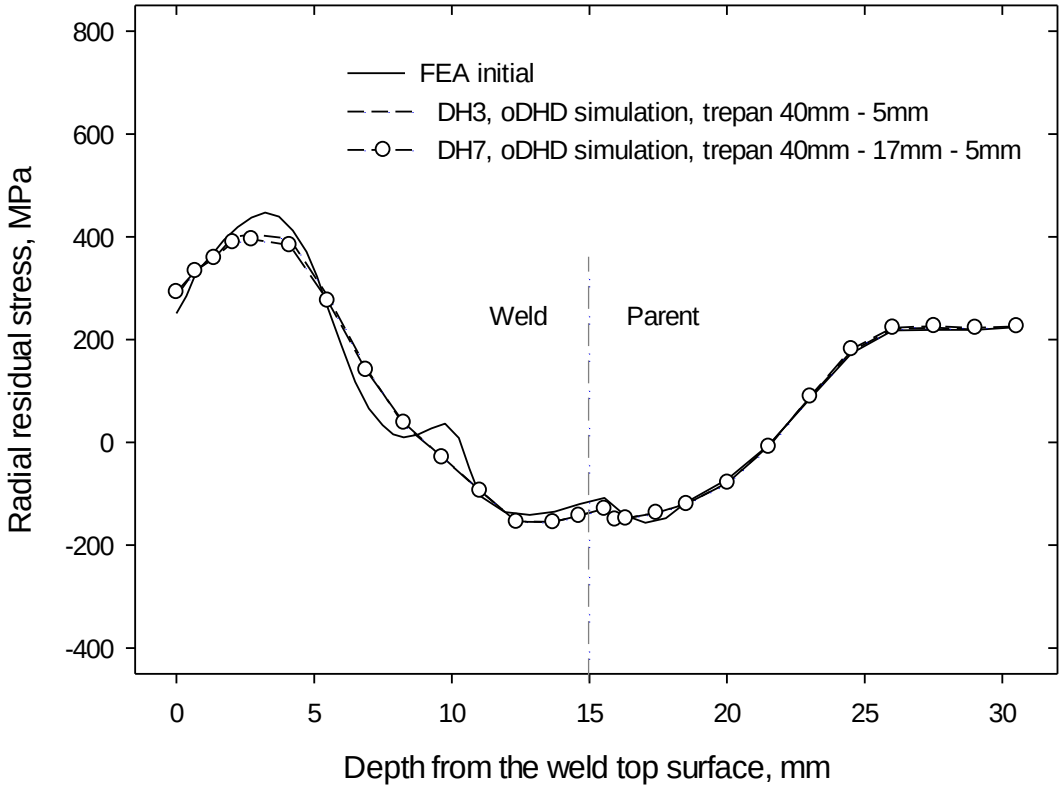

(a) Radial stress

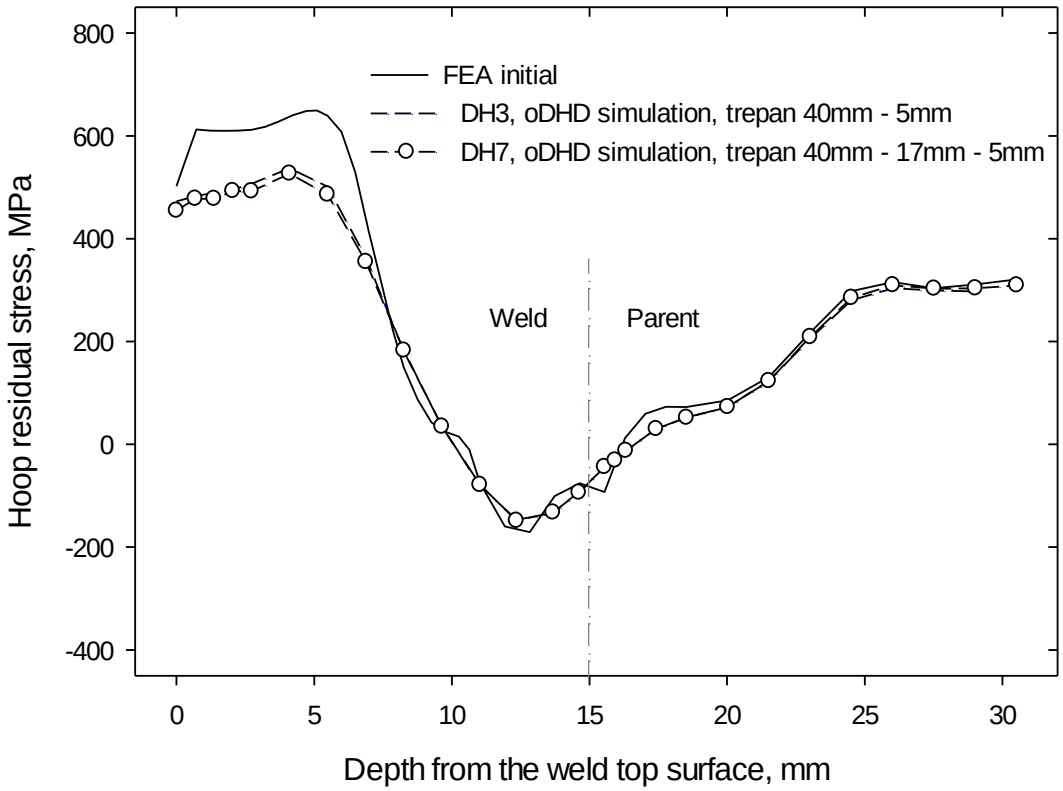

(b) Hoop stress

Figure 23 oDHD simulation parametric study, influence of over-coring procedure

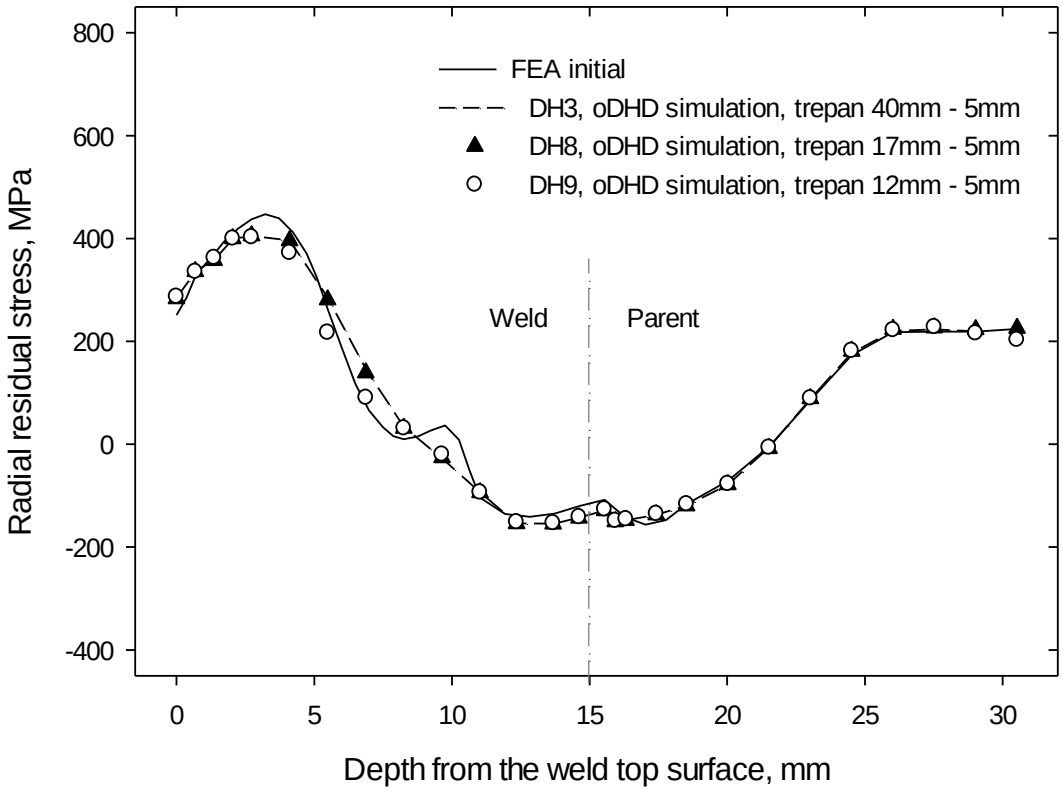

(a) Radial stress

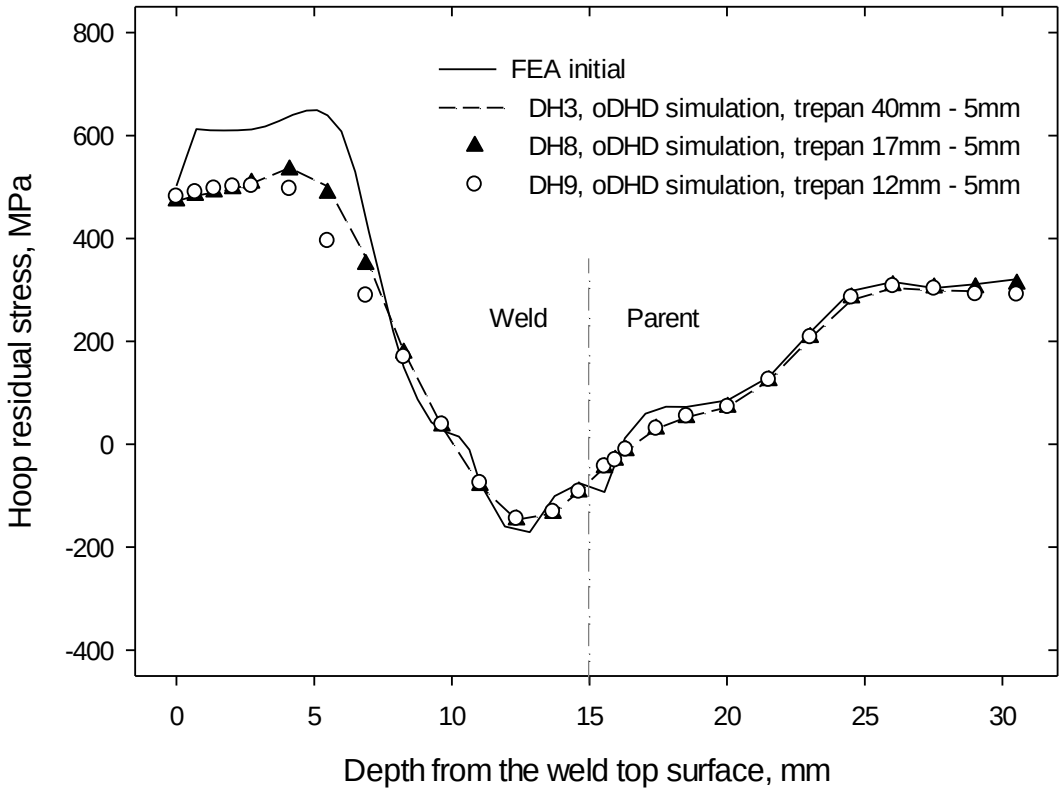

(b) Hoop stress

Figure 24 oDHD simulation parametric study, influence of over-coring size

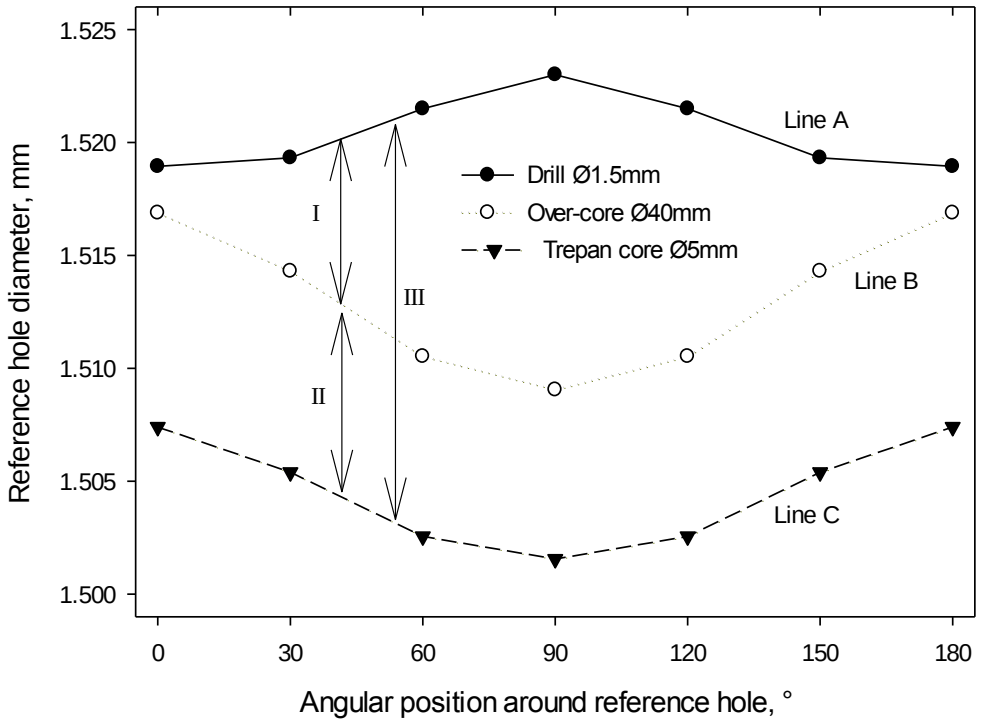

Figure 25 Reference hole diameter at various angles at a selected depth, 4.1mm deep below welded surface

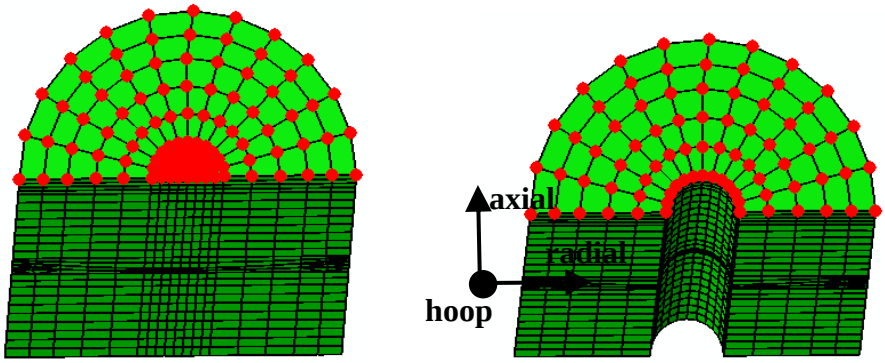

(a) Before drilling (b) after drilling

Figure 26 Node selected for data analysis in Ø5mm core

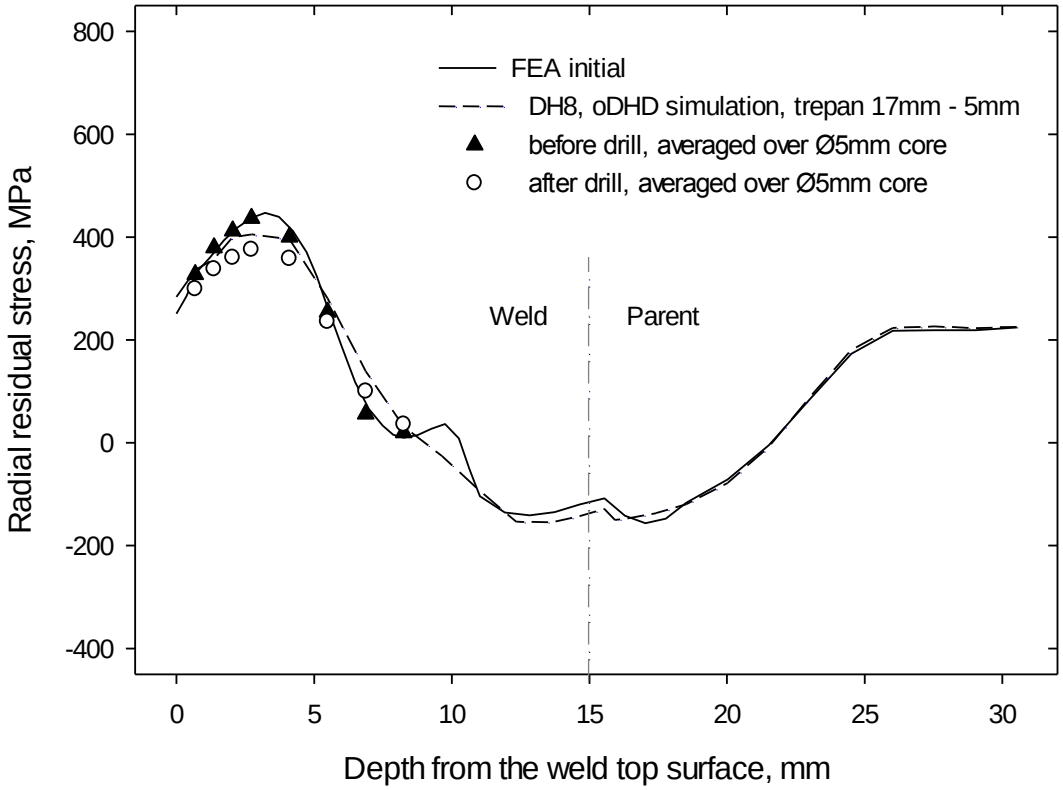

(a) radial

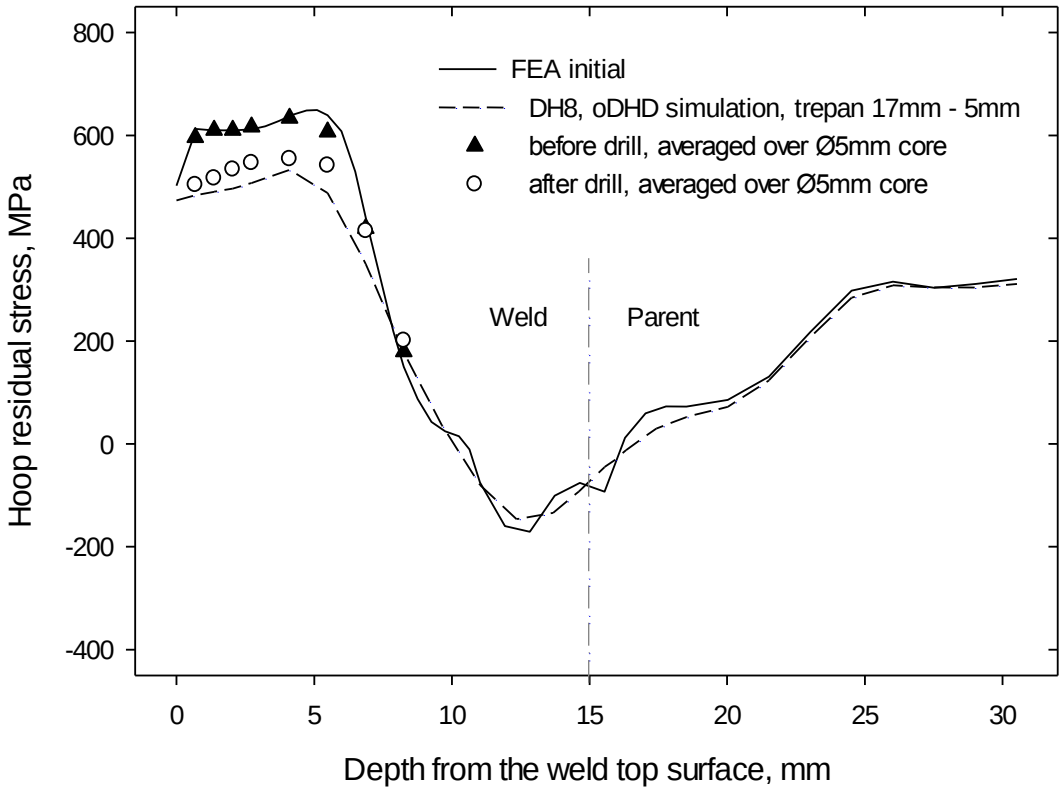

(b)hoop

Figure 27 Stress values comparison among different analysis within Ø17mm core

Vitae

[1, 3] Dr Gang Zheng

Dr Gang Zheng has expertise in stress measurement and prediction (FEA). Gang has obtained his PhD in Mechanical Engineering at the University of Bristol UK under the supervision of Late Prof David J Smith. As part of his PhD research he developed and optimised the measurement of residual stress using deep-hole drilling and neutron diffraction techniques through a combination of experimental and FEA methods. Gang has been working in ENSA (Spain) as project engineer for about three year. He is at present working in the central research institute in State Power Investment Corporation in Beijing China.

[1, 4] Dr Sayeed Hossain

Dr Sayeed Hossain has expertise in residual stress analyses. He has extensive experience in applying Neutron diffraction, X-ray diffraction, Incremental centre-hole drilling, deep-hole drilling and finite element analysis (FEA) methods. Sayeed has worked on numerous projects involving residual stresses, their measurements and their influences on part distortions in aerospace industry and on creep formation in power generation sector. He applied different approach to optimising measurement techniques and advised on the use of FEA concurrent to residual stress measurements for safety critical components. He has worked on construction of VEQTER residual stress database from design and development to implementation stage.

[2] Dr. Ed Kingston

Dr Ed Kingston, co-founder and Managing Director of VEQTER Ltd, first started working on the DHD residual stress measurement technique in 1997 as part of his MEng degree at the University of Bristol. He then continued his research in this field through his PhD, again at the University of Bristol, culminating in the formation of VEQTER Ltd in 2004 with late Prof David Smith. Since then Ed has worked on numerous projects measuring and analysing the residual stresses within engineering components using most of the techniques currently available, be it in VEQTER's lab in the UK or on-site at client facilities around the world.

[1] Prof Christopher E Truman

Prof Christopher E Truman is a Professor of Solid Mechanics in the Department of Mechanical Engineering at the University of Bristol. His research interests are primarily focussed on measuring and modelling residual stress, and fracture of structural materials. The presence of residual stresses can have a significant effect on the subsequent failure characteristics of engineering components and structures. Prof Christopher Truman was an EPSRC Advanced Research Fellow (ARF) until 2010. He is also non-Executive Director of VEQTER Ltd.

[1, 5] Late Prof David J Smith

Late Prof David J Smith was a Royal Academy of Engineering Professor at the University of Bristol (UoB) supported by the Royal Academy of Engineering, EDF-Energy and Rolls Royce. His academic interests lied in fracture of materials and locked-in stresses in engineering components. He was co-Director (with Dr Tom Scott) of the newly formed South West Nuclear Hub at Bristol.

David was a member of the Solid Mechanics Research Group in UoB's Department of Mechanical Engineering, Director of the Systems Performance Centre, and recipient of a Royal Society Research Wolfson Merit Award (2007-2012) and a non-Executive Director of VEQTER Ltd.